ZINC OXIDE NANOPARTICLES AND SH-SY5Y CELL LINE

By

Jinghui Zheng

RECOMMENDED:
Dr. Kriya Dunlap

Dr. Kelly Drew

Dr. Debendra Das

Dr. Lawrence Duffy
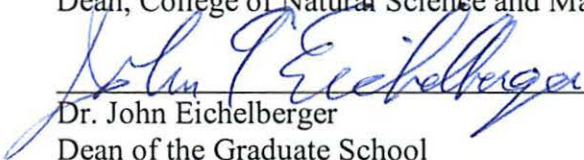Advisory Committee Chair

Dr. William Simpson
Chair, Department of Chemistry and Biochemistry

APPROVED:
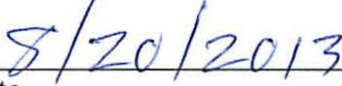Dr. Paul Layer
Dean, College of Natural Science and Mathematics

Dr. John Eichelberger
Dean of the Graduate School

8/20/2013
Date

ZINC OXIDE NANOPARTICLES AND SH-SY5Y CELL LINE

A

THESIS

Presented to the Faculty

of the University of Alaska Fairbanks

in Partial Fulfillment of the Requirements

for the Degree of

Master of Science

By

Jinghui Zheng, B.S.

Fairbanks, Alaska

August 2013

Abstract

The Arctic and sub-arctic regions are impacted by the growth of the global nanotechnology industry. Nanomaterials have unique chemical and physical properties that may lead to toxicological effects that interfere with normal cellular metabolism. Zinc oxide nanoparticles (ZnO NPs) are now very common and widely used in daily life. In industry, ZnO NPs are used to protect different materials from damage caused by UV exposure. The scientific literature suggests that ZnO NPs can have negative impacts on both living organisms and plants. However, there is a paucity of research on the mechanisms by which ZnO NPs may affect the neuronal cells.

This study investigates how ZnO NPs interact with the neuroblastoma cell line SH-SY5Y. Using transmission electron microscopy, we observed that the ZnO NPs form 36 nm particles on average, and increase the level of vascular endothelial growth factor (VEGF) in extracellular fluid, as measured by an enzyme-linked immunosorbent assay (ELISA). Moreover, ZnO NPs, in presence of tumor neucrosis factor- α (TNF-α), can also decrease the level of extracellular VEGF compared with TNF-α treatment alone. These findings suggest the basis for more studies on understanding the mechanism by which ZnO NPs impact cytokine signaling. Another direction is using ELISA technology to observe the interactions of NPs with different cell types such as neuronal stem cells.

Dedication

This thesis is dedicated to my parents and family who have supported and encouraged me throughout my life. I would also like to thank my professors and student colleagues for their assistance and encouragement.

Table of Contents

List of Figures

List of Tables

List of Appendices

List of Abbreviations

CNS	Central nervous system
DI	Deionized
ELISA	Enzyme-linked immunosorbent assay
Ex	Extracellular
FBS	Fetal bovine serum
FICT	Fluorescein isothiocyanate
GLUT4	Glucose transporter type 4
In	Intracellular
IL-1	Interlukin-1
IL-6	Interlukin-6
NP	Nanoparticle
PBS	Phosphate buffered saline
PG	Propylene glycol
PlGF	Placental growth factor
ROS	Reactive oxygen species
RPM	Revolutions per minute
RT	Room Temperature
TEM	Transmission electron microscopy
TNF-α	Tumor neucrosis factor- α
VEGF	Vascular endothelial growth factor
ZnO NPs	Zinc oxide nanoparticles

Acknowledgements

I would like to sincerely express my appreciation to the Department of Chemistry and Biochemistry staff and faculty. Special thanks go to Dr. Lawrence Duffy for his support and patience. Although he is busy with working for UAF Administration, he always had time to discuss my research; he enhanced my critical thinking abilities, encouraged me to design my own experiments, and provided me with his valuable opinions. His educational philosophy earns my sincere respect. I really appreciate his inspiration and guidance.

Another person I want to express my gratitude for is Dr. Kriya Dunlap. She is the person who worked with me on the basic lab techniques of biological assay and cell culture. Her passion about research, as well as her optimism, influences me in a big way.

I would also like to thank my committee member Dr. Kelly Drew for her advice, which played an important role in modifying my experiments' design and inspired me to think more in depth about my research. Dr. Debendra Das provided me with different kinds of nanoparticle materials and encouragement. Without these materials, I would not have been able to conduct my research project. Dr. Ken Severin, although he is not on my committee, gave me lots of help on Transmission Electronic Microscopy.

Chapter 1: Background and Introduction

1.1 Nanoparticles and Zinc Oxide

Nanoparticles (NPs) are particles with a diameter typically smaller than 100 nanometers (nm) that differ from their bulk form (diameter >1000nm) and usually have unique properties. Carbon nanotubes are one of the most widely used nanomaterials. These NPs conduct heat efficiently and have unique electrical properties, as well as distinctive architectures. They are usually composed of many nanotubes bonded together and possess a highly activated surface. Hydroxyapatitie (HA) and carbon-coated titanium alloys are other examples of commonly used NPs. They have been used in bone and hip replacements in the medical field (Yang et al., 2010). NPs are also used in the pharmaceutical field to develop substances for drug delivery (De Jong and Borm, 2008). This is especially true for the anticancer, anti-bacterial and anti-viral drug development industries. Nowadays, researchers find that NPs can be applied to cell-specific targeting of Leukemia and other cancer types and, increasing the diversity of the biotech industry.

Although nanomaterials bring benefits, they also can have negative impacts on the ecosystem and living organisms. The disposing of carbon nanotube batteries can be a problem. If they are not disposed properly, they can move into the ecosystem; be accessed by some living organisms, including humans, via the food chain; and potentially lead to cancer (Buzea et al., 2007). Also, the NPs' unique surface properties (i.e. the charge and the reactivity) can lead to unexpected biological inflammations. Since NPs can pass the blood brain barrier based on their small size (De Jong and Borm, 2008), they

have access to neurons. Several toxicological studies support the contention that airborne

NPs and are correlated with inflammatory effects (De Jong and Borm, 2008,

Dobrovolskaia et al., 2008, Borm et al., 2006).

ZnO NPs, as one of the common metal nanomaterials, have been used in common

products. In the construction industry, ZnO NPs are used to coat wood, plastic or textiles

to protect them from exposure to UV light. In the cosmetic field, ZnO NPs are an

essential element in sunscreens. Although ZnO NPs have enjoyed a good reputation for

their diverse properties, they are rarely studied for their toxicity. Kumari and his team

have found that ZnO NPs can act as clastogenic and cytotoxic agents when NPs contact

with root cells of *Allium cepa* (Kumari et al., 2011). NPs have been found to be toxic not

only in plants cells, but also in animals. Bai et al. (2010) found that ZnO NPs are toxic to

the zebrafish embryos. Specifically, the research found that 30 nm nanoparticles form

aggregates of different sizes during the exposure process. They showed that the exposure

to ZnO NPs induced embryonic mortalities, though, the exposure did not lead to direct

embryonic death. In addition, the high concentration of ZnO NPs and the Zinc ions

decreased the embryos' hatching rate. Exposure to ZnO NPs also shortened the body

length of larvae and induced tail malformation as the concentration increased (Bai et al.,

2010).

1.2 Cytokines

Cytokines are a group of proteins that play an important role in cell signaling. They are secreted by numerous cells, and in particular, immune cells. Upon cell stimulation, some cytokines increase up to 1000-fold in plasma after trauma or infection, and sometimes they are used as biomarkers by clinicians to monitor for infection and inflammation (Hopkins et al., 2012, Kemp et al., 2005, Fava et al., 1994).

Cytokines, such as Interlukin-1 (IL-1) and Tumor Necrosis Factor-α (TNF-α), are involved in the immune response to infection in abnormal cells, and are characterized as pro-inflammatory (Boyle 2005). Production of the pro-inflammatory cytokines has been associated with tumor growth in a variety of neoplasms and neurological disorders (Duffy et al., 2011). The IL-1 family also is important in both acute and chronic inflammation. IL-1 receptor binding induces the activation of transcription factors and the expression of genes that promote the production of other cytokines as well as growth factors, such as vascular endothelial growth factor (VEGF) (Duffy et al., 2011). Two forms of IL-1 exist (IL-1α and IL-1β), which interact with the type I and type II IL-1 receptors. IL-1 binds to the receptor type I and initiates a signaling cascade leading to the activation of the transcription factor, nuclear factor-κB, which is central to inflammatory and immune responses, as well as angiogenesis (Monaco et al., 2004).

VEGF, as mentioned earlier, can be induced by IL-1 during the inflammation. It is also known as vascular permeability factor (VPF) or vasculotropin. VEGF is expressed by numerous rodent and human tumor cells (Kemp et al., 2005). In normal tissue, VEGF expression has been found in activated macrophages (Fava et al., 1994); keratinocyte

4

(Brown et al., 1992b); renal glomerular visceral epithelium and mesangial cells (Brown et al., 1992a, Iijima et al., 1993); hepatocytes (Monacci et al., 1993); smooth muscle cells (Ferrara et al., 1991); embryonic fibroblasts, bronchial, choroid plexus epithelia cells (Pertovaara et al., 1994, Breier et al., 1992) as well as neurons and glial cells (Storkebaum and Carmeliet, 2004).

The occurrence of VEGF/PlGF heterodimers has also been observed in the conditioned media of human choriocarcinoma cells (JAR[*] and JE-3[†]) (Cao et al., 1996), in which PlGF, a protein called placenta growth factor, is one that activates growth factors (Roskoski 2007). In vivo, VEGF can induce angiogenesis, a process that is associated with wound healing, embryonic development, and the growth and metastasis of solid tumors, as well as an increase in microvascular permeability (Kemp et al., 2005). Based on all the factors listed above, VEGF is expected to play an important role in inflammation during pathological angiogenesis. Elevated levels of VEGF have been reported in synovial fluids of rheumatoid arthritis patients and in sera from cancer patients (Koch et al., 1994, Senger et al., 1993, Kondo et al., 1994).

---

[*] JAR: Experimental cell line
[††] JE-3: Experimental cell line

1.3 Flow Cytometry

Flow Cytometry technique was developed during 1970s by a research group at Stanford University and was patented as the first Fluorescence Active Cell Sorter (FACS). In 1974, the first commercial flow cytometer called the FACS-1 was licensed by Becton Dickinson, Inc. During the late 1970's, multi-parameter capability for flow cytometers was developed. During the early 1980's, the first high-speed flow cytometer was successfully used to sort human chromosomes as part of the Human Genome Project. By the end of the 1980's, flow cytometers became the industry-standard commercial cell analyzer (Herzenberg et al., 2002). Nowadays, flow cytometers are employed in various fields, such as academic research, commercial research and clinical diagnoses.

I collaborated with Dr. Dunlap's research group to develop the flow cytometry method to monitor cell populations after treatments involving exercise. Our initial effort was focused on the influence of exercise on measuring the expression of GLUT4 receptors on the membrane of white blood cell populations in sled dogs.

It is intended that this technique will eventually be used to monitor the changes in neuroblastoma and stem cells after exposure to ZnO NPs and other nanoparticles.

1.4 Significance and Research Hypothesis

1.4.1 Significance

The production of engineered nanomaterials in 2004 was 2000 tons and is projected to increase to 58,000 tons by 2020 (Nowack and Bucheli, 2007). However, the unique properties of metal oxide nanomaterials may have a negative impact on the ecosystem.

In this research, we focused on the ZnO NPs because they have been widely used in consumer products such as sunscreens. Kumari (Kumari et al., 2011) and his team reported that ZnO NPs can act as both clastogenic and cytotoxic agents when in contact with root cells of *Allium cepa* (onion bulb). They compared ZnO NPs (size < 100 nm with varying concentrations) with ZnO bulk (size < 5μm with different concentrations) forms. The ZnO NPs increased lipid peroxidation in *A. cepa* cells. Bai and his group observed ZnO NPs were also toxic to the zebrafish embryos, exposure to 50 and 100 mg/L ZnO NPs increased the embryonic mortalities, shortened the body length of larvae, and induced tail malformation when the concentration reached 10 mg/L (Bai et al., 2010). Using these studies as an indicator, it is obvious that researchers should expand studies on the mechanism of ZnO NPs on cell signaling. Our research is an attempt to build a cell culture model that allows for the study of cell-signaling after exposure to NPs as well as facilitate the potential of development of neuro-protective nutraceuticals that can reduce the impact of ZnO NPs exposure.

1.4.2 Research Hypothesis

At the outset of this research, our goals were relatively broad and exploratory in nature. My literature research found no reported studies of NPs effect on SH-SY5Y cells, so as an exploratory study. There are few studies where metallic nanomaterilas have been used to investigate toxicology at the cellular level. Among these few studies, they only reported mortality effect the cells in culture. This exploratory study is the first, to our knowledge, to access the impact of metallic nanomaterials on cytokines like VEGF. For this exploratory research, initial hypotheses were developed, and modified as exploratory results were obtained. Theses hypothesis are:

1. ZnO NPs have a relatively stable size and structure in solution

2. ZnO would not significantly impact the pH of the cell media

3. ZnO NPs are toxic to SH-SY5Y cells alone at defined concentrations (5µl/ml to 10µl/ml)

4. The toxicity of the ZnO NPs can be correlated with the release of extracellular VEGF by SH-SY5Y

5. ZnO NPs will inhibit the effect of TNF-α on SH-SY5Y cells as judged by the release of VEGF into culture media

Chapter 2: Materials and Method

2.1 Human SH-SY5Y Cell Culture

Human SH-SY5Y neuroblastoma cells were grown from the frozen cells, stored in liquid nitrogen, then thawed in to 100-mm dishes (Falcon) containing: high-glucose DMEM (pH 7.4), 10% fetal bovine serum (FBS), 3.7 g/L sodium bicarbonate, 100U/ml of penicillin and streptomycin, and 1% GlutaMax-1 (GM) (Table 2.1). Cultures were incubated in a humidified atmosphere with 5% CO_2 at 37°C. After one week of incubation, cells were detached using 0.5 mg/ml trypsin (5 min, 37°C), collected by centrifugation (1,200 rpm), and plated into six-well plates. After another week of incubation in the six-well plates, the media was replaced with serum-free media. All experiments were carried out 24-hours after serum depriving the neuron cultures.

Table 2.1 Sources of materials used

BCA Protein assay kit	Pierce Biotech
DMEM powder	Mediatech
Fetal Bovine Serum	Atlanta Biologicals
GlutaMax-1	Invitrogen
Human SH-SY5Y neuroblastoma cell	ATCC
Human VEGF assay kit	R&D Systems
IL-1 assay Kit	R&D Systems
Trypsin	Invitrogen
TNF-α assay kit	R&D
SystemsParaformaldehyde	Invitrogen
Penicillin/Streptomycin	Mediatech
Recombinant human TNF-α	ProSpec
RPMI media	Invitrogen
Zinc Oxide nanoparticles (ZnO NPs), 36 nanometer, powder	Alfa Aesar
All other reagents	Sigma-Aldrich

2.1.1 Light Microscopy of SH-SY5Y Cell

After growing for one week in a six-well plate, neuroblastoma cells were observed under the Nikon Eclipse TE 2000U inverted microscope to assess the normal condition of the cells. Morphology changes after the treatments were noted. Normal morphology shows asymmetric cells with processes.

2.1.2 pH Detection in Human SH-SY5Y Cell Media

pH is an important parameter that can alter the cell's viability. Proteins, nucleic acid and lipids need to maintain the interval pH for their normal function such as signal transduction, gene expression and membrane physiology. Changes in hydrogen ion concentrations can impact normal cells' metabolism. pH was measured using the Thermo Orion 420 Plus pH meter after treatments and as well as the blank.

2.2 Human SH-SY5Y Cell Treatments

Cell cultures in six-well plates that were free of microbial contamination were deprived of serum for 24h. The cell cultures were then treated with the following: a) a controlled culture with no treatment, b) a culture with 0.2 µg/ml of ZnO NPs for 4h, c) a culture with 0.4 µg/ml of ZnO NPs for 4h, d) a culture with 0.125 µg/ml TNF-α for 4h, e) a culture with 0.125 µg/ml TNF-α for 30 minutes, and f) a culture with 0.4 µg/ml of ZnO NPs for 4 hours, followed by addition of 0.125 µg/ml TNF-α for 30 minutes. The 6-well plates were incubated in a humidified atmosphere of 5% CO_2 at 37 $^{\circ}$C for either 30 minutes or 4 hours.

2.3 Transmission Electron Microscopy

Transmission Electron Microscopy (TEM, JEOL 1200) was used to detect the morphology characteristics of ZnO NPs. ZnO NPs were dispersed in propylene glycol (PG) in a 1:9 PG ratio (10µl of NPs and 90µl PG) for a 10% final solution. 5µl of prepared ZnO NPs solutions were pipetted on to the TEM grid and after 20s, were blotted off the grid, then 5µl of DI water was placed on the grid for 20s and blotted from the grid. After repeating 3 times, the grid was dried overnight. The grid of ZnO NPs was examined after one day.

2.4 Enzyme-linked Immunosorbent Assay

Enzyme-linked immunosorbent assay (ELISA) is a very powerful biological technique that uses antibody and color change to quantify the substance of interest. The principle for these assays, in general, is that antibodies can specifically bind with certain substances (antigens or hapten). There is a microplate (usually a 96-well plate) which is pre-coated with known antibody specific to the protein of interest. When standards and samples are added into the wells, the substance (antigen or hapten) will bind to the immobilized antibody. Then a secondary antibody with an attached enzyme added to each well; this antibody binds with the antigen. The attached enzyme is reacts with an added secondary substrate, which will finally develop a color change and the data can be detected by an absorbance plate reader. The substance (antigen or hapten) in the samples can be detected both qualitatively and quantitatively.

For VEGF, as a specific example, a monoclonal antibody specific for VEGF has been pre-coated onto a microplate. If VEGF exists in the samples, it will bind to the

immobilized antibody. After 3 repeated, saline washes steps to clear away the unspecific binding, an enzyme-linked polyclonal antibody specific for VEGF is added to the wells. A substrate solution is added after, and then the color develops in proportion to the amount of VEGF in the samples. Final measurements are done by using a plate reader set for λ=450 nm. The concentration of VEGF in the sample is determined by interpolation from a standard curve. The same basic principle and approach is applied in IL-1α assay (Duffy et al., 2011, Kemp et al., 2005).

2.4.1 BCA Protein Assay

The BCA protein assay (Pierce) is commonly used to determine protein content in samples. It is a detergent compatible formulation based on bicinchoninic acid for the colorimetric detection and quantitation for total protein in the samples. The assay is based on the principle that Cu^{2+} is reduced to Cu^{+} by protein in an alkaline medium, which is called the biuret reaction. The reaction is detected with a highly-sensitive and selective colorimetric detection of the Cu^{+} using a unique reagent containing bicinchoninic acid. The final color of the solution will be purple and depends on the concentration of proteins existing in samples. The colors can also appear in different shades. The purple color is caused by the chelation of two molecules of bicinchoninic with one Cu^{+}.

2.4.2 VEGF Assay

The human R and D system VEGF ELISA assay allows measurements of extra and intracellular VEGF from cultured human SH-SY5Y cells. By following published directions (R&D Systems), VEGF was detected in a colorimetric change plate. A Beckman-Coulter Multimode DTX 880 multi-plate reader detected the color change at an

absorbance λ=450nm. For this assay, the lowest detectable concentration of VEGF is 5.0 pg/ml.

After ZnO NPs and TNF-α treatments, the media was directly removed and utilized for the extracellular assay. The same remaining cells were rinsed with PBS. Cells were removed by scraping in ice-cold PBS. The cells were collected in Eppendorf tubes and sonicated for 5 seconds then utilized for the intracellular assay.

2.4.3 IL-1α Assay

The human R and D system IL-1α assay allows measurements of extracellular and intracellular IL-1α from human SH-SY5Y cells. A Beckman-Coulter Multimode DTX 880 multi-plate reader detected the color change at an absorbance λ=450nm.

IL-1α levels were determined for both secreted (extracellular) and cellular (intracellular) concentrations in SH-SY5Y cells after ZnO NPs and TNF-α treatments. The media was directly removed and added to the ELISA plate to detect the extracellular IL-1 level. The same remaining cells were rinsed with PBS. Cells were removed by scraping in ice-cold PBS. The cells were collected in Eppendorf tubes and sonicated for 5 seconds and utilized for the intracellular assay.

2.5 Flow Cytometry

Flow cytometry is a laser-based, biophysical technology employed in cell counting, sorting and biomarker detection. This technique has been commonly used to diagnose health disorders, especially hematological diseases. The principle of sorting particles is based on their different chemical and physical properties. The specific cell

populations can be tagged with specific fluorescent markers in order to separate them from other populations.

In the project, I used FITC that was conjugated to the secondary antibody, in order to target the GLUT4 receptors on the cell membrane and detect the florescent signal by using flow cytometry. The results will show us if there will be different expression levels of GLUT4 receptors on mononuclear cells' membrane from sled dogs measured before exercise, immediately after exercise, and after a recovery period of 24 hours. This research will contribute to develop an improved way to detect blood GLUT4 levels as well as contribute to the development of a low-invasive diagnostic tool for insulin resistance and type II diabetes.

Chapter 3: Results

3.1 Characteristics of Zinc Oxide Nanoparticles

The characterization of ZnO NPs was critical at the outset of this research. The size and shape of the ZnO NPs was detected and observed using TEM machine at several magnifications. One result shows that ZnO NPs tended to form aggregates in aqueous environments under 100,000 magnification, which is consistent with other ZnO NPs morphology studies (Figure 3.1).
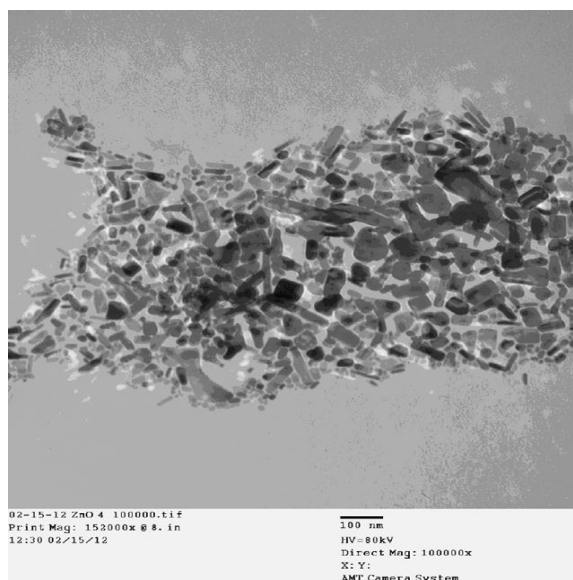
Figure 3.1 ZnO NPs morphology under 100,000X

The ZnO NPs tended to form aggregates; but most individual particle's size is still smaller than 100nm. Figure 3.2 suggests that any effects of ZnO to cell cultures will be caused by its "Nano" form, not its "Fine" form in which particle diameters is between 100nm and 1000nm, or its "Bulk" form in which particle diameter is larger than 1000nm.
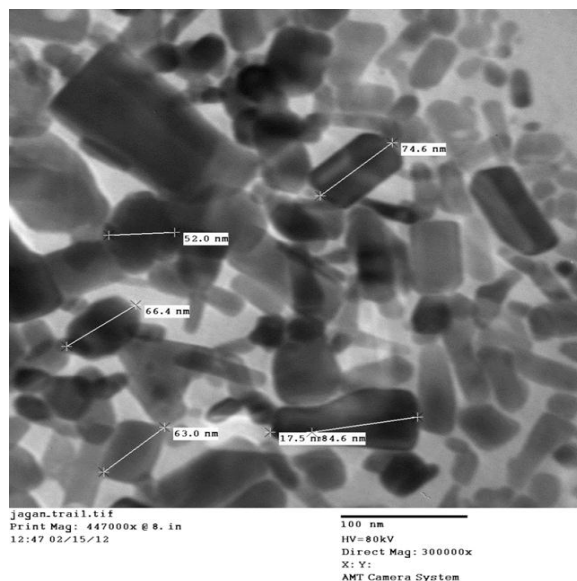
Figure 3.2 ZnO NPs morphology under 300,000X

Figure 3.3 shows the general morphology of ZnO NPs under the 500,000 magnification. ZnO NPs do not show a clearly-defined shape. They can be observed as three types: oval shape, rectangular-elongated shape and round shape. The darker color of ZnO NPs in Figure 3.3 indicated that ZnO NPs are overlapping each other. When magnification was expanded, the definition of these elongated ZnO NPs was more evident and the average size was estimated to be 36nm.

The particles exist within a narrow range size. Generally speaking, individual particle diameter is smaller than 100nm and particles tend to aggregate in aqueous environment. All these characteristics can be important for their interactions with SH-SY5Y cells.
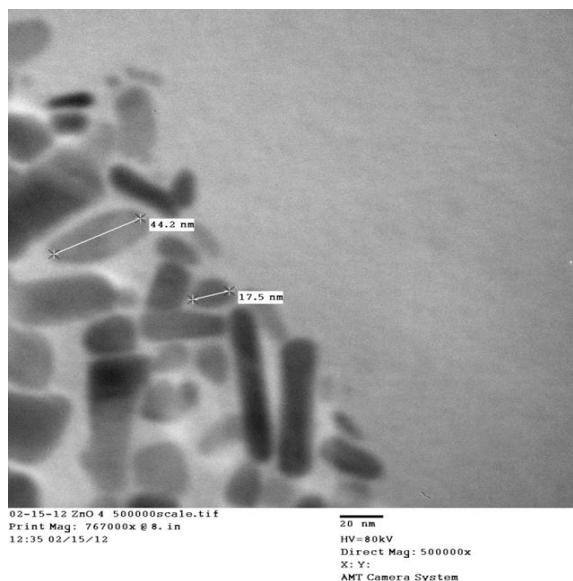
Figure 3.3 ZnO NPs morphology under 500,000X

3.2 Acid-Base Cell Culture Environment

The hydrogen ion concentration (pH) is an important cell culture parameter that can alter the cells' viability. Altering the pH of cell media (living environment) can alter the behavior of proteins, nucleic acid, lipids and other important molecules' normal function. Maintaining pH in a defined range is required for cells to perform their normal metabolic activity.

ZnO is known to be an amphoteric oxide, whether the cell media pH was changed after the addition of the ZnO NPs was recorded by using a Thermo Orion 420 Plus pH meter (Table 3.1).

Table 3.1 pH changes of cell culture media after treatments

Sample	Concentration (ZnO NPs/TNF-α)	pH	Difference between no treatment and treatments
No Treatment	0.00 µg/ml	6.94	———
ZnO NPs	0.20 µg/ml	6.99	0.05
ZnO NPs	0.40 µg/ml	7.01	0.07
ZnO NPs	0.80 µg/ml	7.07	0.13
TNF-α	0.125 µg/ml	7.19	0.25

We compared the difference in pH for at the listed concentrations (Table 3.1) of
ZnO NPs and TNF-α treatments used in these experiments with no treatment, the average
difference in pH between ZnO NPs treatments and no treatment is 0.08. The TNF-α, is
used throughout the study, because it shows a positive release of VEGF into the media,
also had an impact on the pH on the media. The difference between TNF-α treatment and
no treatment was 0.25.

3.3 Cell Viability

3.3.1 Light Microscopy of Human SH-SY5Y Cell

The standard shape of SH-SY5Y cells in culture is well-defined (Gustafson et al., 2012). The morphology of SH-SY5Y cells under 20X magnification after 24h (in a serum-free media) demonstrates that the cells remain healthy. The cells maintain their projections and shape. This illustrates the nomal morphology of the cells before treatments in a serum-free media (Fig 3.4).
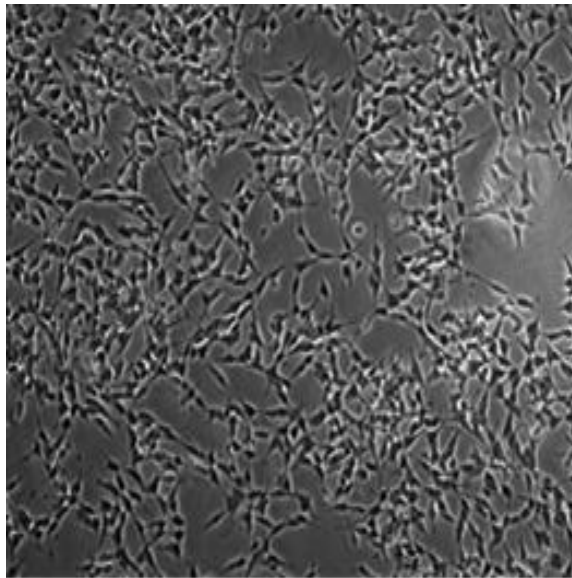
Figure 3.4 SH-SY5Y in serum free cell culture

3.3.2 Impact of ZnO NPs on SH-SY5Y Cell

Our results showed that high concentration of ZnO NPs, which is 0.80 µg/ml (equals 20µl added to cell media) over 24 hours resulted in the complete mortality of the cells. A series of concentration and time-dependent experiments were used to define conditions for observing impacts of low concentrations of ZnO NPs.

Figure 3.5 shows the morphology of SH-SY5Y under 20X after 1 hour of 0.4 µg/ml ZnO NPs treatment. The morphology changed distinctly. The numbers of axon projection were reduced, and many cells changed morphology to a rounded shape.
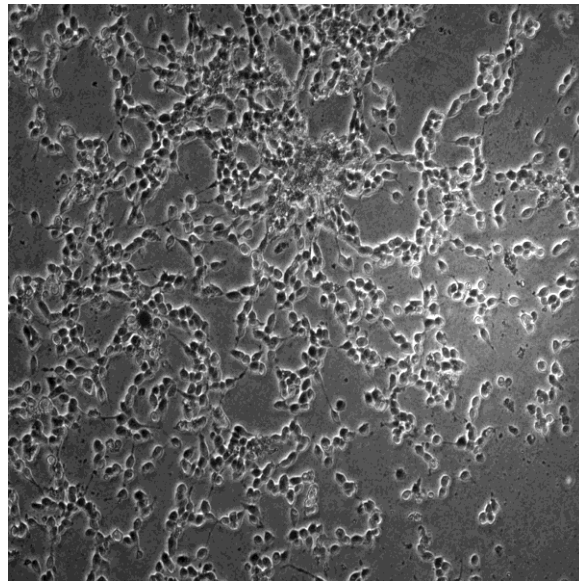
Figure 3.5 SH-SY5Y in ZnO NPs exposure (1h)

After 4h, the morphology of SH-SY5Y of 0.40 µg/ml ZnO NPs treatment showed that most cells lost their normal morphology and axon projections. There was almost complete disappearance of connectivity between cells (Fig 3.6).
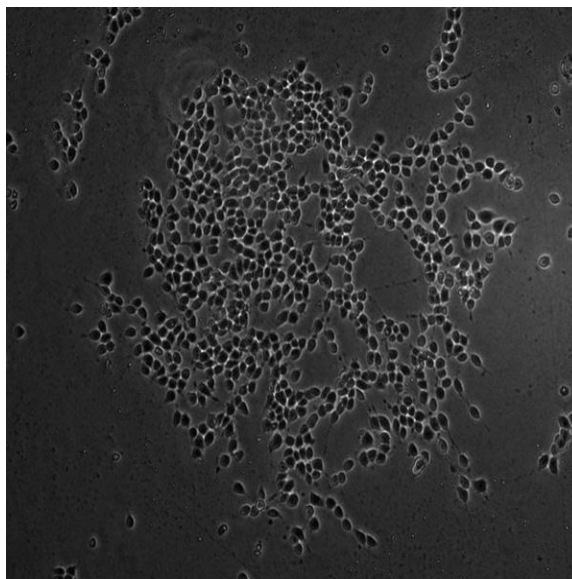
Figure 3.6 SH-SY5Y cell culture in ZnO NPs exposure (4h)

3.4 ZnO NPs and VEGF Secretion

As mentioned in the hypothesis section, we expected to see that ZnO NPs treatments cause an increased release of extracellular VEGF. The results of the ELISA assay for VEGF support this hypothesis.

The results showed that 0.4 µg/ml of ZnO NPs a for 4h exposure treatment increased the extracellular VEGF concentration. However, the VEGF level in ZnO NPs treatment was less than the TNF-α treatment under the same time period exposure. The ZnO NPs treatment showed 160 pg/ml VEGF while TNF-α showed 450 pg/ml.
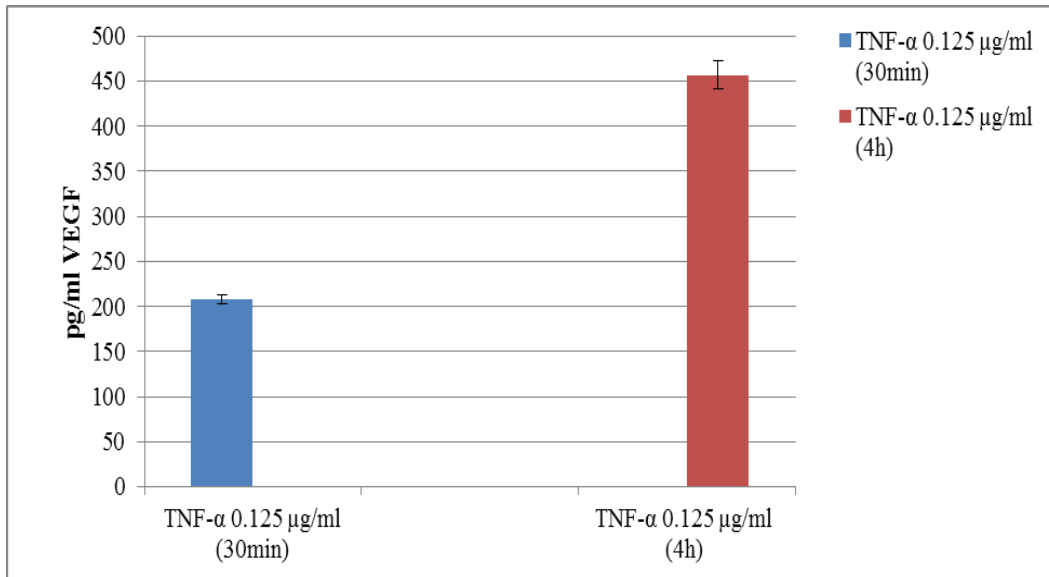
Figure 3.7 VEGF extracellular releases after TNF- α

Figure 3.7 shows that, after different incubation times with 0.125 µg/ml of TNF-α, the level of VEGF extracellular release is different depending on length of the exposure. The level of VEGF in the media after a 4h incubation is almost two times that of the sample after a 30-minute incubation. This is expected because the longer the exposure time the more the VEGF will be released into the culture. This data shows that VEGF release under the TNF-α stimulation is a time-dependent behavior, the longer the exposure time, the more VEGF been induced. This data also shows the responsiveness of the cells. TNF-α is a positive control in our treatment. These results are also consistent with previously reported results, for a 30-minute TNF-α incubation that can increase the extracellular VEGF level (Duffy et al., 2011). The VEGF level in the sample without TNF-α treatment was under the detectable level. Since this is only one trail ran in triplicates, statistics were not performed, although this explored the issue of whether exposure length could impact VEGF levels in future studies.
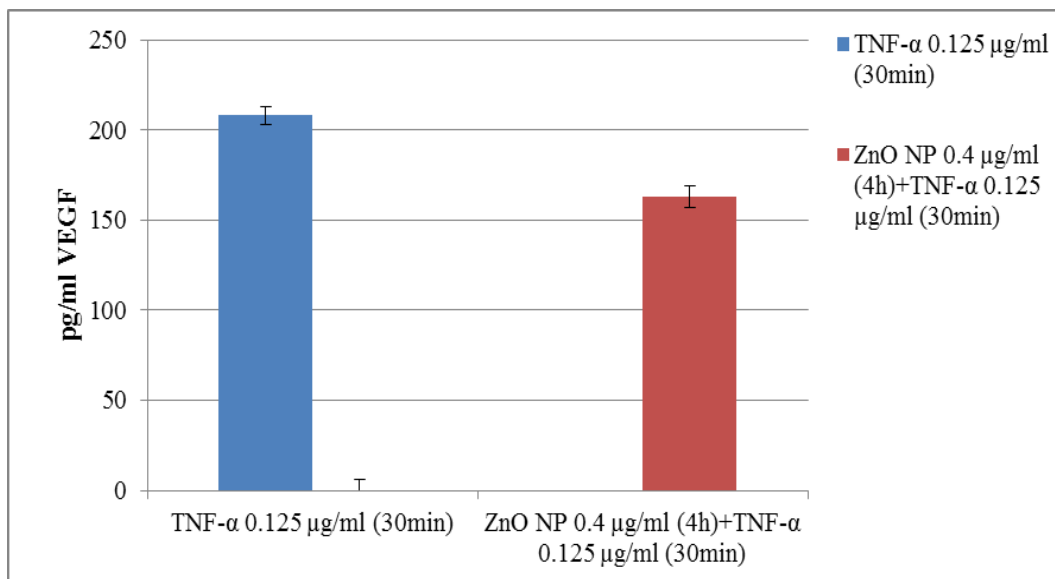
Figure 3.8 VEGF extracellular releases after combining TNF-α and ZnO NPs

Figure 3.8 shows extracellular VEGF concentration after treatment of ZnO NPs (0.4 µg/ml) followed by a 30-minute TNF-α (0.125 µg/ml) treatment. The 30-minute TNF-α (0.125 µg/ml) treatment is shown as a baseline stimulation. This result showed that the level of VEGF release after TNF-α (0.125 µg/ml) treatment is higher than in ZnO NPs (0.4 µg/ml) for 4h and followed by a 30-minute TNF-α (0.125 µg/ml) treatment. An explaination for this result is that ZnO NPs supressed the level of TNF-α induced VEGF release. An alternative explanation is that ZnO NPs killed the cells, reducing the number of cells that can release VEGF. The second explanation is supported by the light microscopy result shown in Fig 3.6, in which there is a decreased number of cells in the two ZnO NPs treat wells (Table 3.2). This can be interpreted that ZnO NPs killed cells so they could not emit VEGF. The reduced amount of protein detected by the BCA protein assay indicated the reduced number of cells. Since only duplicates performed in the experiment, these results are not significant and should be verified by repeated trails in

the future. Repeated trails will also allow us to address the significance of the difference in protein levels between longer and shorter ZnO NPs exposure periods.

The effects of stressors, either cytokines or toxicants, can be additive, subtractive or synergistic. Figure 3.8 show that in the effect of ZnO NPs+TNF-α appears subtractive.

Table 3.2 BCA protein assay

samples	No Treatment	ZnO 0.4 µg/ml (30min)	ZnO 0.4 µg/ml (4h)	TNF-α 0.125 µg/ml (30min)
1	0.085	0.061	0.075	0.096
2	0.097	0.060	0.067	0.083
AVE	0.090	0.061	0.071	0.090
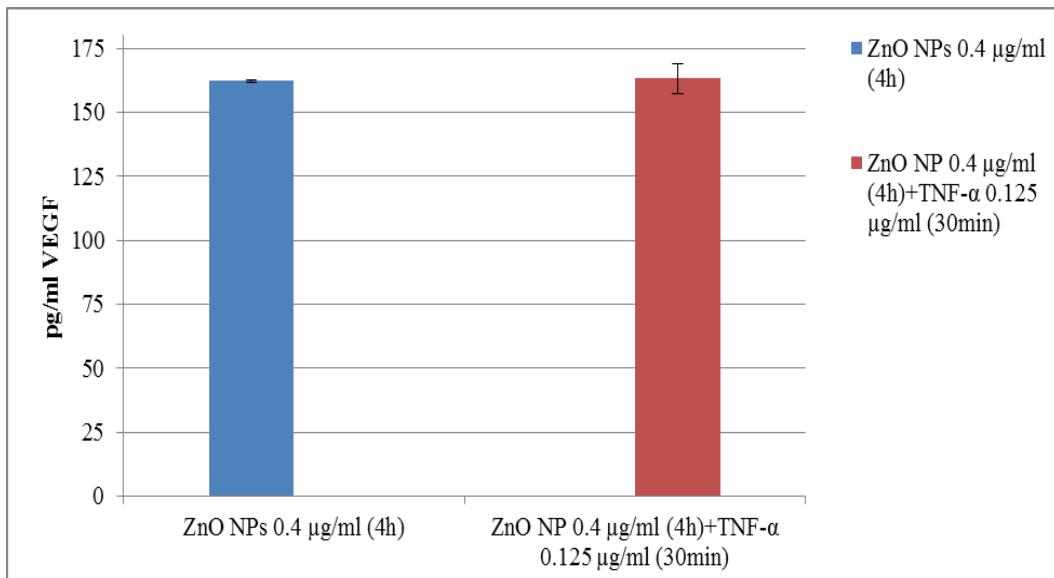
Figure 3.9 VEGF extracellular releases after combining ZnO NPs and TNF-α

blank showed under detectable level of VEGF

Figure 3.9 shows that after 4h treatment with ZnO NPs (0.4 µg/ml) alone and with TNF-α (0.125 µg/ml, 30 minutes after 4h ZnO NPs treatment), there was no difference in extracellular VEGF. This result shows that pretreatment of ZnO NPs does not directly enhance the TNF-α induction of VEGF, and may inhibit it.

3.5 ZnO NPs affects IL-1α

Interleukins are a large group of proteins produced mainly by T-cells and in some cases by mononuclear phagocytes. Most interleukins direct other cells to divide and differentiate. Interleukins largely participate in the regulation of immune response, as well as inflammation and hematopoiesis. Each acts on a specific group of cells that have receptors specific to an interleukin.

IL-1 is a name and designation for two proteins, IL-1α and IL-1β, which are the products of distinct genes. Both of these proteins recognize the same cell surface receptors. IL-1 is usually not produced by healthy individuals, except in skin keratinocytes, some epithelial cells, and certain cells in the central nervous system (Dinarello and Wolff, 1993). A dramatic increase in the production of IL-1 is commonly detected after stimulation by inflammatory agents or microbial endotoxin. In this project, IL-1 was also investigated, however, there was no difference between the control and ZnO NPs' treatment. All but the TNF-α control sample were below detectable levels.

Chapter 4: Discussion and Future Directions

ZnO NPs have been used in many products. Previous studies (Bai et al., 2010) show that the aggregation effects can increase the toxicity of ZnO NPs. TEM results in this research show that ZnO NPs (size=36nm, 4% in PG) aggregate in solution and the average size of the particles is about 36nm. Moreover, these particles do not have a definite shape and therefore they can potentially affect cells differently. However, there is no reported research on neuronal cells and cytokines are usually not studied. Some researchers revealed that nanoparticles could be shaped to fit to particular proteins, and have important interactions with complement proteins (Dobrovolskaia et al., 2008). In addition, researchers shows that the smaller the size of nanoparticles, the more toxic they are (Kumari et al., 2011, Bruneau et al., 2013).

TNF-α and IL-1 have primary roles in the regulation of immune cells through NF-κB signaling pathway, and contribute to the adaptive immunity and secretions of pro-inflammatory cytokines (Janeway et al., 1999). VEGF is a signal protein that is produced by numerous types of cells. VEGF can stimulate new blood vessels and lymphatic vessels to grow under normal conditions. When VEGF is over-expressed, it can contribute to diseases, especially cancer. In advanced cancer studies, researchers create VEGF-receptors antagonists to block the VEGF production in tumor cells. This is under development as a potential cancer therapy (Kerbel, 2000).

Our research reveals that after 4h incubations with ZnO NPs, the normal morphology of SH-SY5Ycells disappear. They lose their projections of axons and the interactions with nearby cells. The ELISA results show that ZnO NPs with a

concentration of 0.4 µg/ml increased the extracellular VEGF production by about 160

pg/ml after 4h incubation. On the same plate, the VEGF in the blank (no treatment) was

below the detectable limits (5 pg/ml). In comparison, using exposure to TNF-α with a

concentration of 0.125 µg/ml, which increased the extracellular VEGF production by

about 450 pg/ml after 4h incubation with the ZnO NPs, has a lesser effect on extracellular

VEGF production compared with TNF-α treatments alone. In addition, we studied the

double-effects of ZnO NPs and TNF-α to SH-SY5Y cells. The results show that the

extracellular VEGF production is almost the same under ZnO NPs and ZnO NPs+TNF-α

conditions. And the ZnO NPs+TNF-α treatment has fewer effects on extracellular VEGF

production (160 pg/ml) than the TNF-α treatment alone (450 pg/ml). This result has two

possible explanations: 1) the ZnO NPs can inhibit the releasing of VEGF in the presence

of TNF-α, which can be used in a potential cancer drug development, or 2) the ZnO NPs

killed the cells before they could release more VEGF into media. The second explanation

is supported by both the image result (Fig 3.6) and BCA protein result (Table 3.2). In

addition, the results from the ELISA also show that the effects of ZnO NPs on the SH-

SY5Y cells may also be through the pathway leading to VEGF secretion. The ZnO NPs

do not induce the releasing of IL-1α according to this research.

Figure 4.1 shows a schematic diagram summarizing the results from the ELISA,

and suggesting the ZnO NPs may interfere with the TNF-α regulating pathway. This

interference leads to reduction in the TNF-α-stimulated release of VEGF.
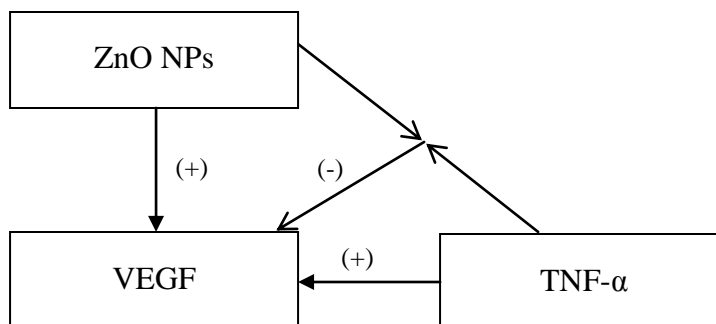
Figure 4.1 Diagram shows the pathway involved in ZnO NPs, VEGF and TNF-α

This research is in the preliminary stage of developing a model system. Future experiments will be required to better understand what effects ZnO NPs have on neuronal cells. I suggested the following studies to be conducted

1) The permeability of ZnO NPs through biological membranes

2) The aggregation effect of ZnO NPs on cells

3) Whether ZnO NPs will affect the release of other cytokines such as IL-4 and IL-10, inhibitory cytokines that are capable of inhibiting synthesis of pro-inflammatory cytokine such as TNF-α.

There are many questions that need to be answered about characterization of ZnO NPs and neuronal cells. Answering these questions will be crucial to regulating the fast growing nanotechnology industry.

As described in Appendix B, another future direction of this project will be the use of flow cytometry to sort different populations of cells and study the ZnO NPs' effects on the cell viability and molecular expression in immune cells.

The research in this thesis was exploratory in nature. We performed numerous experimental trials, some of which did not work as expected, and through this experimentation, we discovered how to improve the design and what were key factors

and components to pay attention to. Since many of these tests were only performed in one or two trials, we did not perform standard statistical analyses of the results. Future work would include more trials so as to demonstrate the statistical significance of the results. This exploratory research gave us preliminary results that help us to design cell culture experiments to understand the effect of ZnO NPs exposure on VEGF secretion in SH-SY5Y cells.

Chapter 5: Literature Cited

Bai, W.; Zhang, Z.; Tian, W.; He, X.; Ma, Y.; Zhao, Y.; Chai, Z., Toxicity of Zinc Oxide
Nanoparticles to Zebrafish Embryo: A Physicochemical Study of Toxicity
Mechanism. *J Nanopart Res.* **2010,** *12 (5),* 1645-1654.

Borm P.J.; Robbins D.; Haubold S.; Kuhlbusch T.; Fissan H.; Donaldson, K.; Schins, R.;
Stone, V.; Kreyling, W.; Lademann, J.; Krutmann, J.; Warheit, D.; Oberdorster,
E., The Potential Risks of Nanomaterials: A Review Carried for ECETOC.
Particle and Fibre Toxicology **2006,** *3 (11).*

Boyle, J. J. Macrophage Activation in Atherosclerosis: Pathogenesis and Pharmacology
of Plaque Rupture. *Curr Vasc Pharmacol* **2005,** *3 (1),* 63-68.

Breier, G.; Albrecht, U.; Sterrer, S.; Risau, W., Expression of Vascular Endothelial
Growth Factor During Eembryonic Angiogenesis and Endothelial Cell
Differentiation. *Development* **1992,** *114 (2),* 521-532.

Brown, L. F.; Berse, B.; Tognazzi, K.; Manseau, E. J.; Van de Water, L.; Senger, D. R.;
Dvorak, H. F.; Rosen, S., Vascular Permeability Factor mRNA and Protein
Expression in Human Kidney. *Kidney international* **1992a,** *42 (6),* 1457-61.

Brown, L. F.; Yeo, K. T.; Berse, B.; Yeo, T. K.; Senger, D. R.; Dvorak, H. F.; van de
Water, L., Expression of Vascular Permeability Factor (Vascular Endothelial
Growth Factor) by Epidermal Keratinocytes during Wound Healing. *The Journal
of Experimental Medicine* **1992b,** *176 (5),* 1375-1379.

Bruneau, A.; Fortier M.; Gagne F.; Gagnon C.; Turcotte P.; Tayabali A., Size
Distribution Effects of Cadmium Tellurium Quantum Dots (CdS/CdTe)

Immunotoxicity on Aquatic Organisms. *Environ. Sci.: Processes Impacts* **2013,** *15,* 596.

Buzea, C.; Blandino, I.; Robbie K., Nanomaterials and Nanoparticles: Sources and Toxicity. *Biointerphases* **2007,** *2 (4),* 17-172.

Cao, Y.; Chen, H.; Zhou, L.; Chiang, M.-K.; Anand-Apte, B.; Weatherbee, J. A.; Wang, Y.; Fang, F.; Flanagan, J. G.; Tsang, M. L.-S., Heterodimers of Placenta Growth Factor/Vascular Endothelial Growth Factor Endothelial Activity, Tumor Cell Expression, and High Affinity Binding to Flk-1/KDR. *Journal of Biological Chemistry* **1996,** *271 (6),* 3154-3162.

De Jong, W. H.; Borm, P. J., Drug Delivery and Nanoparticles:Applications and Hazards. *Int J Nanomedicine* **2008,** *3 (2),* 133-49.

Dinarello, C. A.; Wolff, S. M., The Role of Interleukin-1 in Disease. *New England Journal of Medicine* **1993,** *328 (2),* 106-113.

Dobrovolskaia, M. A.; Aggarwal, P.; Hall, J. B.; McNeil, S. E., Preclinical Studies to Understand Nanoparticle Interaction with The Immune System and Its Potential Effects on Nanoparticle Biodistribution. *Molecular pharmaceutics* **2008,** *5 (4),* 487-95.

Duffy, L.K., Nicholas F.L., Dunlap L.K., Involvement of Cytokine IL-1Ra in Regulating the Secretion of VEGF in SH-SY5Y Neuroblastoma. *International Journal on bioinformatics and biotechnology* **2011,** *1 (1),* 2251-3159.

Fava, R. A.; Olsen, N. J.; Spencer-Green, G.; Yeo, K. T.; Yeo, T. K.; Berse, B.; Jackman, R. W.; Senger, D. R.; Dvorak, H. F.; Brown, L. F., Vascular Permeability

Factor/Endothelial Growth Factor (VPF/VEGF): Accumulation and Expression in Human Synovial Fluids and Rheumatoid Synovial Tissue. *J Exp Med* **1994,** *180 (1),* 341-6.

Ferrara, N.; Winer, J.; Burton, T., Aortic Smooth Muscle Cells Express and Secrete Vascular Endothelial Growth Factor. *Growth factors* **1991,** *5 (2),* 141-8.

Fluorophores.org. http://www.fluorophores.tugraz.at/substance/25 (accessed 2011).

Gustafson, S. J.; Dunlap, K. L.; McGill, C. M.; Kuhn, T. B., A Nonpolar Blueberry Fraction Blunts NADPH Oxidase Activation in Neuronal Cells Exposed to Tumor Necrosis Factor-Alpha. *Oxidative medicine and cellular longevity*, **2012,** 768101.

Herzenberg, L. A.; Parks, D.; Sahaf, B.; Perez, O.; Roederer, M., The History and Future of The Fluorescence Activated Cell Sorter and Flow Cytometry: A View From Stanford. *Clinical chemistry* **2002,** *48 (10),* 1819-27.

Hopkins, S.; McMahon, C.; Singh, N.; Galea, J.; Hoadley, M.; Scarth, S.; Patel, H.; Vail, A.; Hulme, S.; Rothwell, N.; King, T.A.; Tyrrell, J.P., Cerebrospinal Fluid and Plasma Cytokines After Subarachnoid Haemorrhage: CSF Interleukin-6 May be an Early Marker of Infection. *Journal of Neuroinflammation* **2012,** *9:255.*

Iijima, K.; Yoshikawa, N.; Connolly, D. T.; Nakamura, H., Human Mesangial Cells and Peripheral Blood Mononuclear Cells Produce Vascular Permeability Factor. *Kidney international* **1993,** *44 (5),* 959-66.

Janeway, A.C.; Travers P.; Walport M.; Shlomchik J. M., The Immune System in Health and Disease. *Immunobiology*, 4th ed.; New York: Garland Science, 1999.

Kemp, W. S.;, Reynolds, J.A.; Duffy, L. K., Gender Differences in Baseline Levels of Vascular Endothelial Growth Factor in the Plasma of Alaskan Sled Dogs. *American Journal of Biochemistry and Biotechnology* **2005,** *1 (2),* 111-114.

Kerbel, S.R., Tumor Angiogenesis: Past, Present and the Near Future. *Carcinogenesis* **2000,** *21 (3),* 505-515.

Koch, A. E.; Harlow, L. A.; Haines, G. K.; Amento, E. P.; Unemori, E. N.; Wong, W. L.; Pope, R. M.; Ferrara, N., Vascular Endothelial Growth Factor. A Cytokine Modulating Endothelial Function in Rheumatoid Arthritis. *Journal of immunology* **1994,** *152 (8),* 4149-56.

Kondo, S.; Asano, M.; Matsuo, K.; Ohmori, I.; Suzuki, H., Vascular Endothelial Growth Factor/Vascular Permeability Factor is Detectable in The Sera of Tumor-bearing Mice and Cancer Patients. *Biochimica et Biophysica Acta* **1994,** *1221 (2),* 211-4.

Kumari, M.; Khan, S. S.; Pakrashi, S.; Mukherjee, A.; Chandrasekaran, N., Cytogenetic and Genotoxic Effects of Zinc Oxide Nanoparticles on Root Cells of Allium cepa. *Journal of hazardous materials* **2011,** *190 (1-3),* 613-21.

Monacci, W. T.; Merrill, M. J.; Oldfield, E. H., Expression of Vascular Permeability Factor/Vascular Endothelial Growth Factor in Normal Rat Tissues. *The American journal of physiology* **1993,** *264 (4 Pt 1),* C995-1002.

Monaco, C.; Andreakos, E.; Kiriakidis, S.; Mauri, C.; Bicknell, C.; Foxwell, B.; Cheshire, N.; Paleolog, E.; Feldmann, M., Canonical Pathway of Nuclear Factor Kappa B Activation Selectively Regulates Proinflammatory and Prothrombotic Responses in Human Atherosclerosis. *Proc Natl Acad Sci* **2004,** *101 (15),* 5634-9.

Nowack, B.; Bucheli, D.T., Review: Occurrence, Behavior and Effects of Nanoparticles in the Environment. *Environmental Pollution* **2007,** *150,* 5-22.

Pertovaara, L.; Kaipainen, A.; Mustonen, T.; Orpana, A.; Ferrara, N.; Saksela, O.; Alitalo, K., Vascular Endothelial Growth Factor is Induced in Response to Transforming Growth Factor-Beta in Fibroblastic and Epithelial Cells. *Journal of Biological Chemistry* **1994,** *269 (9),* 6271-6274.

Roskoski, J. R., Vascular Endothelial Growth Factor (VEGF) Signaling in Tumor Progression. *Oncology/Hematology* **2007,** *62*, 179–213.

Senger, D. R.; Van de Water, L.; Brown, L. F.; Nagy, J. A.; Yeo, K. T.; Yeo, T. K.; Berse, B.; Jackman, R. W.; Dvorak, A. M.; Dvorak, H. F., Vascular Permeability Factor (VPF, VEGF) in Tumor Biology. *Cancer metastasis reviews* **1993,** *12 (3-4),* 303-24.

Storkebaum, E.; Carmeliet, P., VEGF: A Critical Player in Neurodegeneration. *The Journal of clinical investigation* **2004,** *113 (1),* 14-8.

Yang, Z.; Liu, Z. W.; Allaker, R. P.; Reip, P.; Oxford, J.; Ahmad, Z.; Ren, G., A Review of Nanoparticle Functionality and Toxicity on The Central Nervous System. *Journal of the Royal Society, Interface* **2010,** *7 Suppl 4*, S411-22.

Appendix A Supplementary Data

Table A.1 Corresponds to Figure 3.7

VEGF (pg/ml)	TNF-α 0.125 μg/ml (30min)	TNF-α 0.125 μg/ml (4h)
R1	202.53	481.35
R2	204.00	427.12
R3	217.58	461.58
AVE (n=3)	208.04	456.68
SD (+/-)	4.79	15.85

Table A.2 Corresponds to Figure 3.8

VEGF (pg/ml)	TNF-α 0.125 µg/ml (30min)	ZnO NP 0.4 µg/ml (4h) TNF-α 0.125 µl/ml (30min)
R1	202.54	174.65
R2	204.00	160.12
R3	217.58	154.50
AVE (n=3)	208.04	163.09
SD (+/-)	4.79	6.01

Table A.3 Corresponds to Figure 3.9

VEGF (pg/ml)	ZnO NPs 0.4 µg/ml (4h)	ZnO NP 0.4 µg/ml (4h) TNF-α 0.125 µg/ml (30min)
R1	162.92	174.65
R2	161.77	160.12
R3	161.92	154.50
AVE (n=3)	162.21	163.09
SD (+/-)	0.36	6.01

Appendix B Developing Flow Cytometry on Cells

Demonstration of Different Cell Populations in Sled Dogs Mononuclear cells

Flow Cytometry is a very powerful tool for researchers to study different cell populations. In order to sort out different populations in Flow Cytometry, researchers usually tag fluorochromes on antibodies. In this study, the antibody has been conjugated with the fluorochrome, FITC. Fluorescein isothiocyanate (FITC) is a derivative of fluorescein. It has excitation and emission spectrum peak wavelengths of approximately 495 nm/519nm which shows in the range of green color (Fluorophores.org).

In this particular project, we are interested in studying the effects of exercise on GLUT4 receptor expression levels on white blood cell membranes. GLUT4 (glucose transporter type 4) is the insulin-regulated glucose transporter. It exists abundantly in adipose tissues, and skeletal and cardiac muscle. The fat cells and muscle are two major tissues in the body that respond to insulin. Studying the impact of exercise on expression levels of GLUT4 is crucial to obtain a better knowledge of Type 2 Diabetes (insulin resistant diabetes).

Sled dogs are the model animal for this study. We monitored three different conditions of the dogs' mononuclear cells samples:

1. Sled dogs before exercise, pre

2. Sled dogs after exercise, t=0

3. Sled dogs 24 hours after exercise, t=24h

8 dogs were used for the 3 different conditions (for each condition, n=8), and their mononuclear cells samples were monitored under the flow cytometer after each condition.

Methods

Fixation

1. Collect cells by centrifuge (at the speed of 3600 RPM/1500g) and aspirate supernatant

2. Re-suspend cells in 3ml of 2% paraformaldehyde in PBS

3. Fix for 10min at 37°C

Staining

1. Block in 2-3ml of incubation buffer (dissolve 0.5g bocine serum albumin in 100ml 1X PBS) for 10 min at RT

2. Centrifuge and re-suspend in primary antibody (5µg/ml in 3% BSA/PBS)

3. Incubate 30 min at RT

4. Rinse with 2 ml/sample incubation buffer by centrifuge at 300 RCF for 15 min

5. Re-suspend cells in flurochrome-conjugated secondary antibody diluted in incubation buffer (1:200 dilution in 3% BSA/PBS)

6. Incubate for 30 min at RT

7. Rise with incubation buffer

8. Re-suspend cells in 3ml/sample 1% BSA/PBS

9. Aliquot 1ml of sample into Eppendorf vials
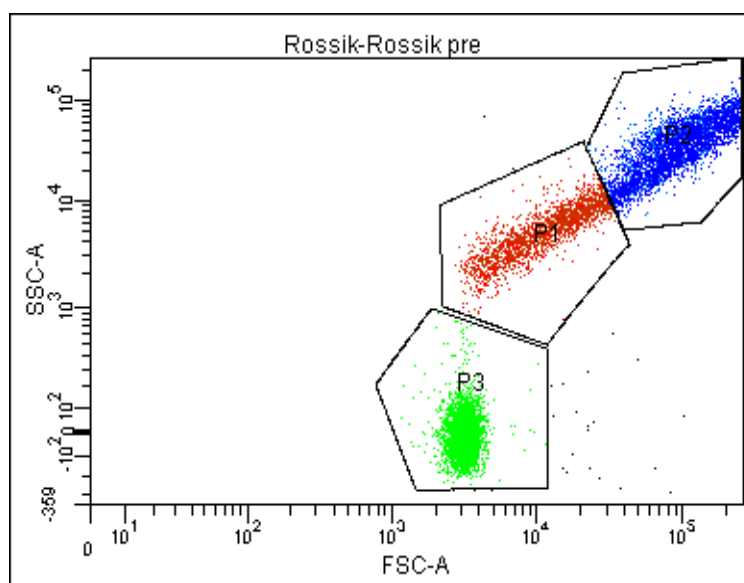
10. Analyze on flow cytometer

Results

Figure B.1 Dot plot for Rossi pre-exercise

Experiment Name: sled dog blood sample
Specimen Name: Rossik
Tube Name: Rossik pre
Record Date: Mar 28, 2013 9:21:53 PM
$OP: Administrator
GUID: 636ee74d-2fb6-4b51-b3e2-b2cd51ea850f

Population	#Events	%Parent	FSC-A Mean	SSC-A Mean	FITC-A Geo Mean
■ All Events	10,000	####	68,706	29,744	####
■ P1	2,066	20.7	13,709	5,789	####
■ P1'	1,215	58.8	14,098	5,950	5
■ P2	4,670	46.7	138,796	61,111	####
■ P2'	3,125	66.9	149,695	66,546	10
■ P3	3,251	32.5	3,154	-7	####

Figure B.2 Experiment data corresponds to Figure B.1

In Figure B.1, the X-axis (FSC-A) represents the overall size of the individual cell,

the Y-axis (SSC-A) represents the complexity or the granularity of the cells. From the dot

plot, the data shows that there are three different populations in the Rossi pre-exercise

white blood samples, and similar results are also found in the other 7 dogs. The 3 different populations were grouped based on their different sizes and granularity. P3 (showns in green) has the smallest size and the least complexity among all the 3 populations. P2 (showns in blue) has the biggest size and the most complexity among all the 3 populations. At this early stage, our prediciton on these three populations will be: P1 is the monocyte, P3 is the lymphocyte. However, furture experiment is needed to verify these populations by tagging markers specific to cell subpopulations.

In Figure B.2, data shows the number of events (corresponding to the number of different types of cells) that were collected. For all the 8 dogs (except the dog Alice-pre), a total of 10,000 events were collected. Data shows that among all the events, P1 has 2066 events (20.7%), P2 has 4670 events (46.7%) and P3 has 3251 events (32.5%). For the FITC Geo Mean (which corresponds to the expression level of GLUT4, standardized to the dogs baseline values), P2 has a higher level of FITC signal compared with P1. The number, respectively, are 5 and 10. And P3 does not has a significant FITC signal.
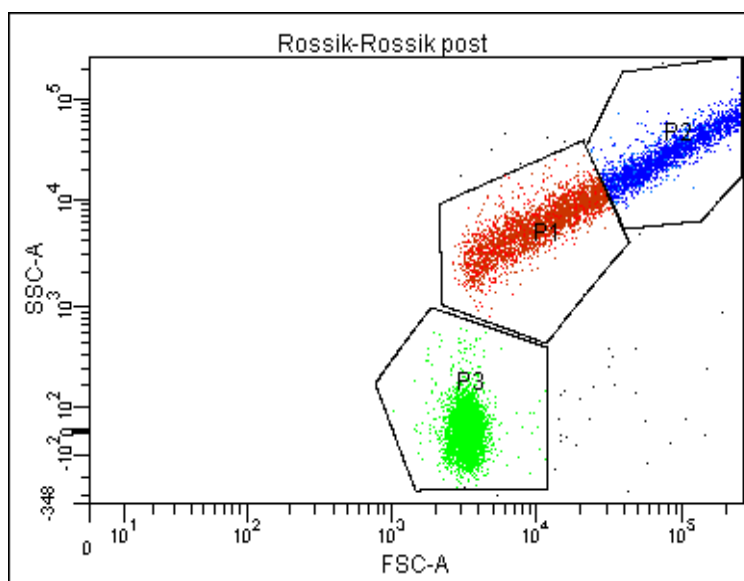
Figure B.3 Dot plot for Rossi post-exercise

Figure B.4 Experiment data corresponds to Figure B.3

Data from Figure B.4 shows that in the Rossi's post exercise white blood sample,

among all the 10,000 events, that P1 has 2826 events (28.3%), P2 has 2954 events

(29.5%) and P3 has 4186 events (41.9%). For the FITC Geo Mean, P2 has a higher level

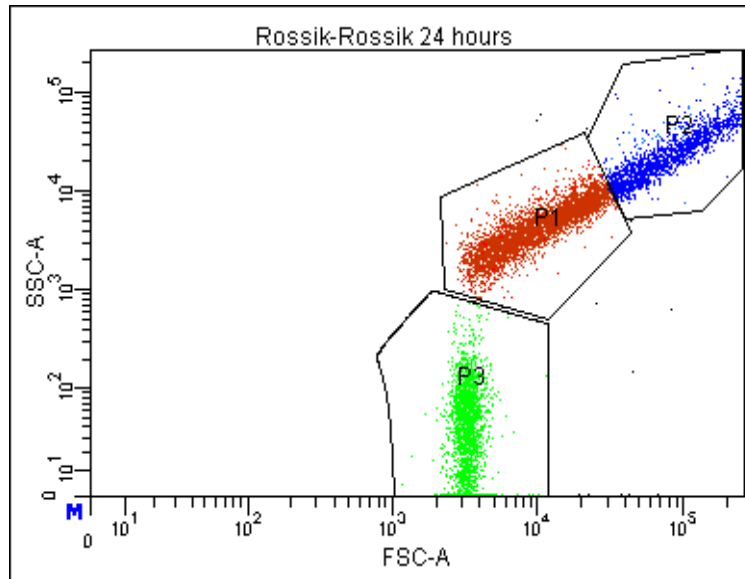of FITC signal compared with P1. The numbers, respectively, are 5 and 15.

Figure B.5 Dot plot for Rossi 24h-post exercise

Experiment Name: sled dog blood sample
Specimen Name: Rossik
Tube Name: Rossik 24 hours
Record Date: Mar 28, 2013 7:57:23 PM
$OP: Administrator
GUID: db33f5d9-9528-438a-9619-9f1d7552611e

Population	#Events	%Parent	FSC-A Mean	SSC-A Mean	FITC-A Geo Mean
All Events	10,000	####	29,822	10,339	####
P1	3,726	37.3	11,894	4,860	####
P1'	3,211	86.2	12,491	5,039	11
P2	2,060	20.6	116,460	41,368	####
P2'	1,987	96.5	116,612	40,690	63
P3	4,206	42.1	3,289	-3	####

Figure B.6 Experiment data corresponds to Figure B.5

Data from Figure B.6 shows that in THE Rossi 24-post exercise white blood

sample, among all the 10,000 events, that P1 has 3726 events (37.3%), P2 has 2060

events (20.6%) and P3 has 4206 events (42.1%). For the FITC Geo Mean, P2 has a stronger signal compare with P1. The numbers, respectively, are 11 and 63.

Overall, under the 3 different conditions, the white blood samples show these following trends in all 8 dogs:

1. There is an increasing number of events in P1

2. There is a decreasing number of events in P2

3. There is no event change in P3

4. There is an increase in FITC signal in P2, which can indicate the increasing expression level of GLUT4 on the membrane of P2
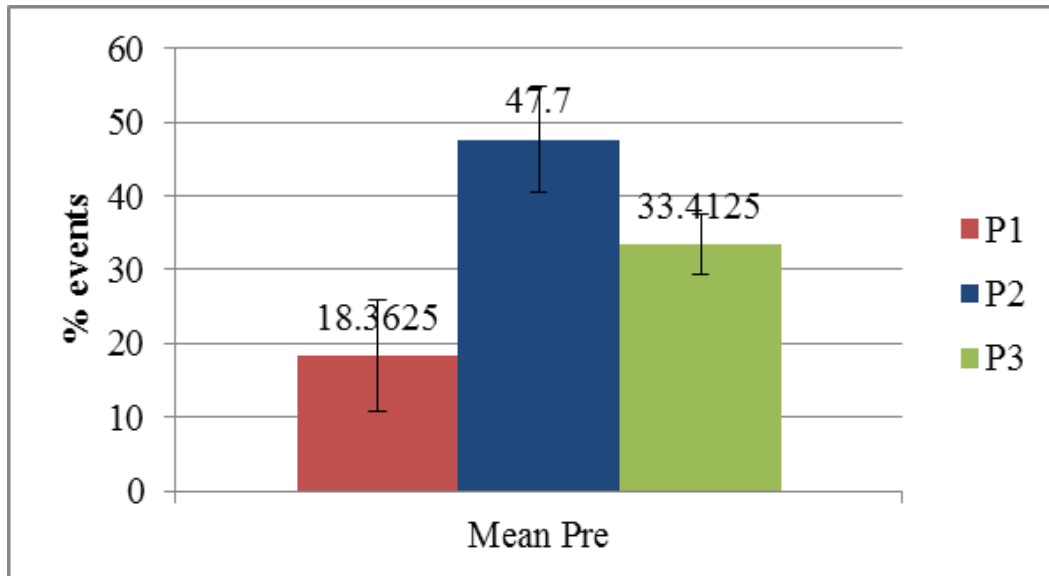
Figure B.7 Mean percentage of events of all three populations in pre-exercise

Table B.1 Corresponds to Figure B.7

Population	Mean Pre (%)	StdDev Pre (+/-)
P1	18.40	7.50
P2	47.70	7.20
P3	33.40	4.10

Figure B.7 shows that in the pre-exercise. Among all the dogs, the P2 has the highest percentage of all three populations followed by P3 and then P1.
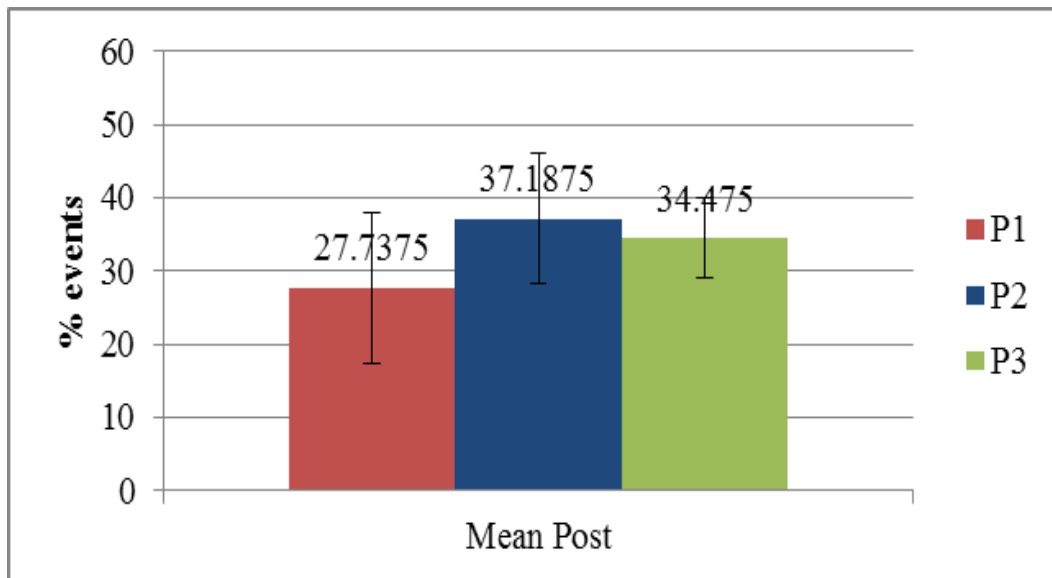
Figure B.8 Mean percentage of events of all three populations in post-exercise

Table B.2 Corresponds to Figure B.8

Population	Mean Post (%)	StdDev Post (+/-)
P1	27.70	10.27
P1	37.20	8.86
P3	34.50	5.50

Figure B.8 shows the post exercise data. Among all the dogs, the percentages events of P1, P2 and P3 do not show a difference.
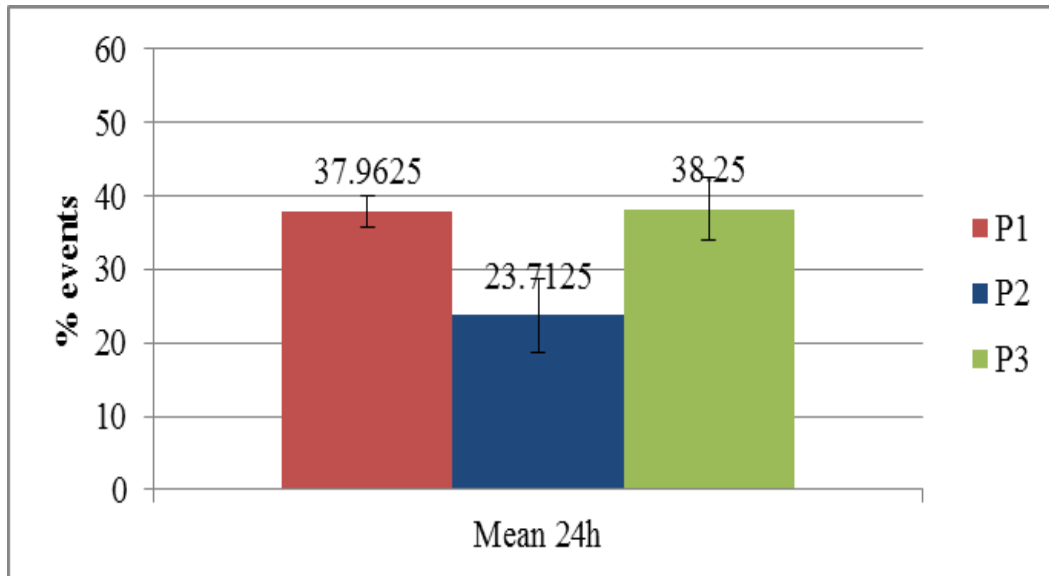
Figure B.9 Mean percentage of events of all three populations in 24h-post exercise

Table B.3 Corresponds to Figure B.9

Population	Mean 24h (%)	StdDev 24h (+/-)
P1	38.00	2.10
P2	23.70	4.90
P3	38.30	4.40

Figure B.9 shows the 24h-post exercise. Among all the dogs, P1 and P3 have the two highest percentages of all the populations, but no difference between these two populations. P2 has the lowest percentage of all the populations.
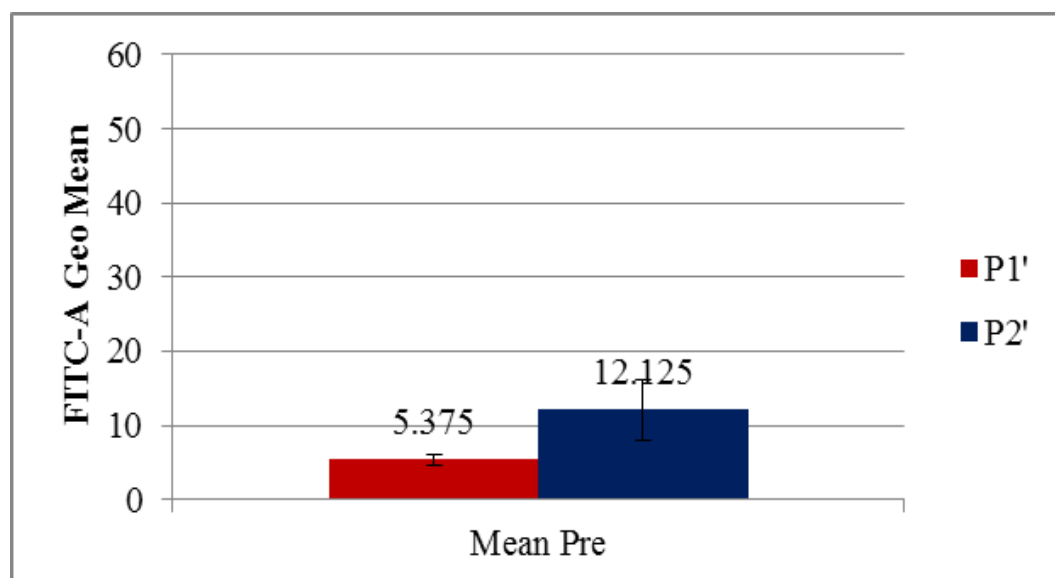
Figure B.10 FITC Geo Means in P1' and P2' populations in pre-exercise

Table B.4 Corresponds to Figure B.10

Population	FITC Geo Mean Pre	StdDev Pre (+/-)
P1'	5.40	0.70
P2'	12.10	4.10

Figure B.10 shows the FITC Geo Mean in P1' and P2' in pre-exercise. Among all 8 dogs, P2' has a stronger signal of FITC compared with P1'. The P1' and P2' are the subpopulations of P1 and P2 separately. These subpopulations do not include the FITC readings that are smaller than 0 (based on the mathematics rule that Geo Mean can only be calculated for the numbers that are bigger than zero).
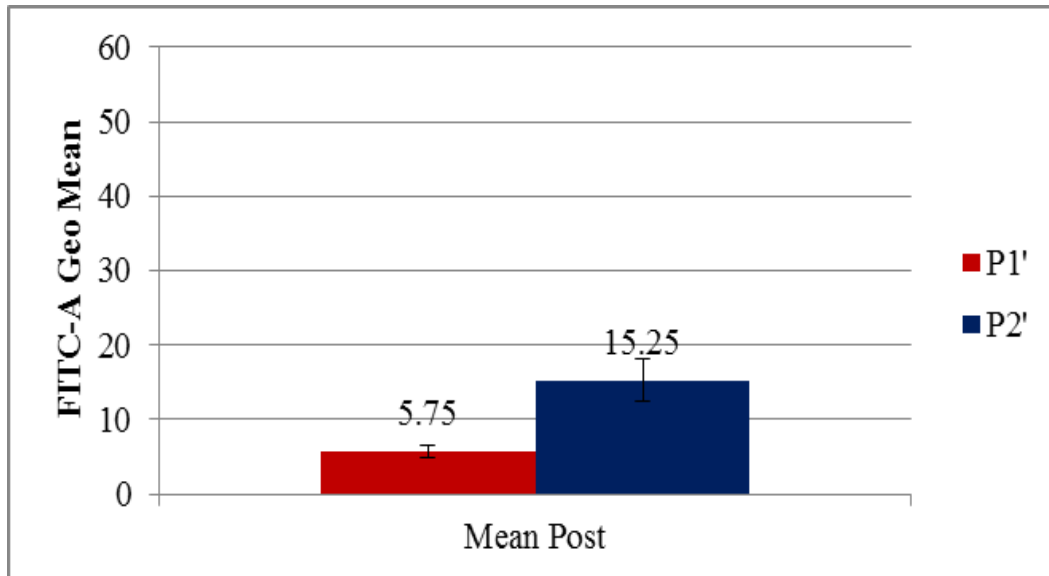
Figure B.11 FITC Geo Means in P1' and P2' populations in post-exercise

Table B.5 Corresponds to Figure B.11

Population	FITC Geo Mean Post	StdDev Post (+/-)
P1'	5.80	0.90
P2'	15.30	2.90

Figure B.11 shows the FITC Geo Mean in P1' and P2' in post-exercise. Among all 8 dogs, P2' has a stronger signal of FITC compared with P1'. In addition, compared with the Pre-FITC Geo Mean reading in P2', Post-FITC Geo Mean in P2' is higher, and there is no change in P1' FITC Geo Mean in both conditions.
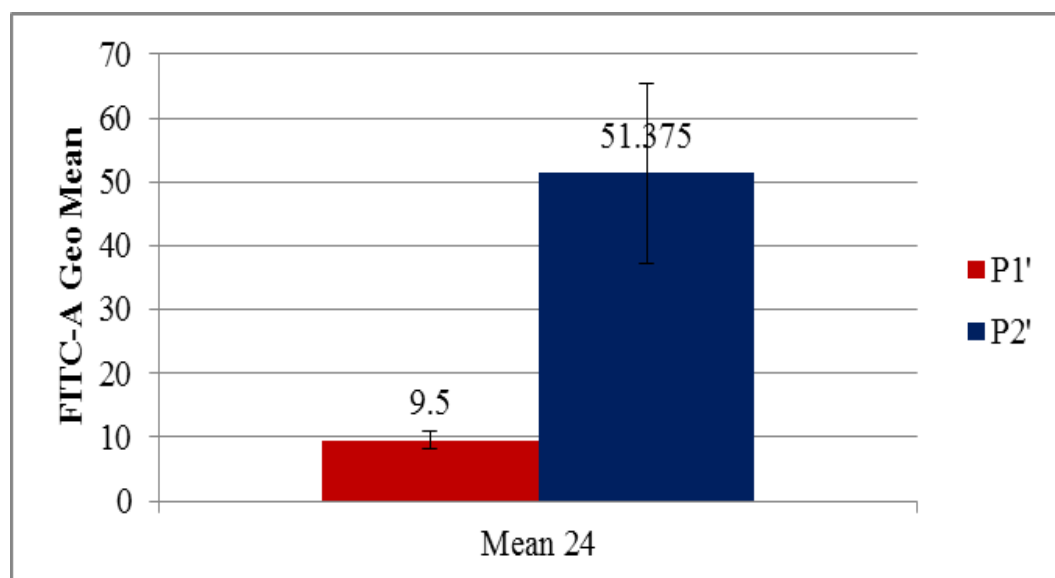
Figure B12 FITC Geo Means in P1' and P2' populations in 24h-post exercise

Table B.6 Corresponds to Figure B12

Population	FITC Geo Mean 24h	StdDev 24h
P1'	9.50	1.30
P2'	51.40	14.10

Figure B.12 shows the FITC Geo Mean in P1' and P2' in 24h-post exercise data. Among all 8 dogs, P2' has a stronger signal of FITC compared with P1'. Compared to the pre-exercise and post-exercise readings, the P2' has the strongest FITC signal among all the three conditions by an increase of about 3 times compared to the pre-exercise and about 2 times compared to the post-exercise.

Conclusion

  From the dot plots collected from Flow Cytometry, our results show cell-population changes in mononuclear cells of sled dogs. There was an increasing in P1 and a decreasing in P2. In order to verify the identity of different mononuclear cells, we will use specific antibodies to tag our samples in future experiments.

  From tagging GLUT4, there is an increasing level of GLUT4 throughout the experiment, from pre-exercise, post-exercise, to 24h-post exercise in P2. This tendency indicates that exercise in sled dogs stimulates the GLUT4 expression on the plasma membranes of mononuclear cell. This finding can be very useful for both academic research on type II diabetes and insulin resistance, but also the potential clinical applications for diagnosis of type II diabetes. The use of blood samples instead of biopsies from adipose or muscle tissue, promise to relatively low-invasive and inexpensive diagnostic tool for determining GLUT4 levels in individuals.

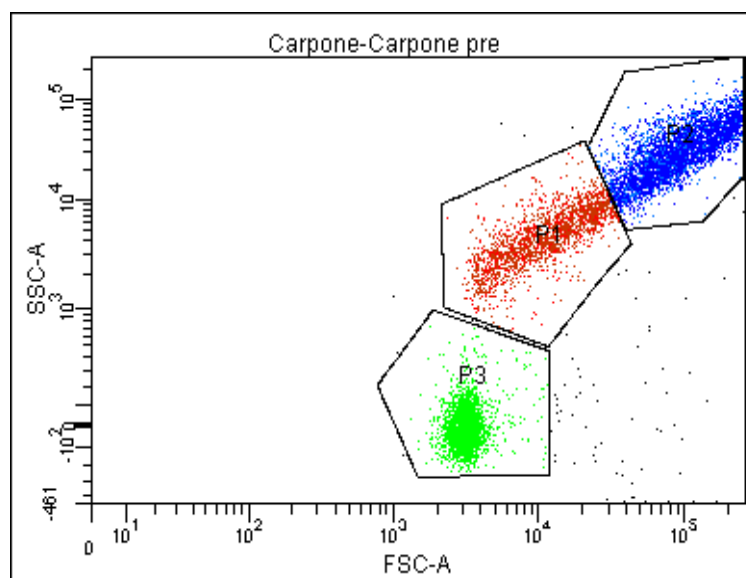**Appendix C Supplementing Data from Sled Dogs Mononuclear cells**

Figure C.1 Dot plot for Carpone pre-exercise

Experiment Name: sled dog blood sample
Specimen Name: Carpone
Tube Name: Carpone pre
Record Date: Mar 28, 2013 8:22:01 PM
$OP: Administrator
GUID: 2bc93ff7-b1e1-4f95-b10b-222af5225530

Population	#Events	%Parent	FSC-A Mean	SSC-A Mean	FITC-A Geo Mean
■ All Events	10,000	####	78,551	32,989	####
■ P1	1,955	19.6	13,315	5,209	####
■ P1'	1,101	56.3	13,543	5,274	5
■ P2	5,137	51.4	145,376	62,208	####
■ P2'	3,280	63.9	157,891	70,500	10
■ P3	2,835	28.3	3,216	-7	####

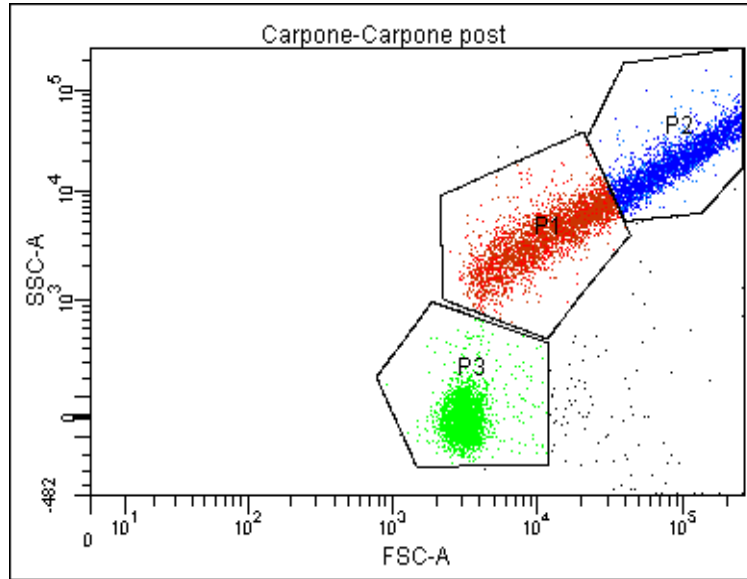**Figure C.2 Experiment data corresponds to Figure C.1**

Figure C.3 Dot plot for Carpone post-exercise

Experiment Name: sled dog blood sample
Specimen Name: Carpone
Tube Name: Carpone post
Record Date: Mar 28, 2013 8:23:28 PM
$OP: Administrator
GUID: bd55f4cc-9f00-4b3c-8d11-9d7d7051f5f4

Population	#Events	%Parent	FSC-A Mean	SSC-A Mean	FITC-A Geo Mean
■ All Events	10,000	####	63,552	22,574	####
■ P1	3,084	30.8	14,182	4,499	####
■ P1'	1,606	52.1	14,375	4,548	7
■ P2	3,773	37.7	153,007	56,100	####
■ P2'	2,837	75.2	166,608	63,596	21
■ P3	3,048	30.5	3,221	-4	####

Figure C.4 Experiment data corresponds to Figure C.3
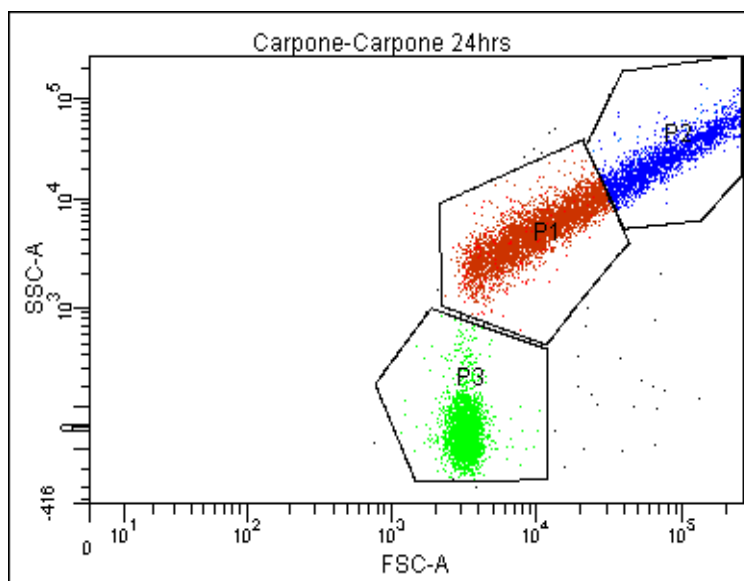
Figure C.5 Dot plot for Carpone 24h-post exercose

Population	#Events	%Parent	FSC-A Mean	SSC-A Mean	FITC-A Geo Mean
■ All Events	10,000	####	38,671	16,273	####
■ P1	4,098	41.0	11,800	5,529	####
■ P1'	3,511	85.7	12,286	5,699	9
■ P2	2,630	26.3	124,359	53,184	####
■ P2'	2,555	97.1	124,841	53,085	59
■ P3	3,239	32.4	3,224	-13	####

Experiment Name: sled dog blood sample
Specimen Name: Carpone
Tube Name: Carpone 24hrs
Record Date: Mar 28, 2013 8:42:09 PM
$OP: Administrator
GUID: a10f5190-37e6-4ba4-bbba-df11b098edba

Figure C.6 Experiment data corresponds to Figure C.5
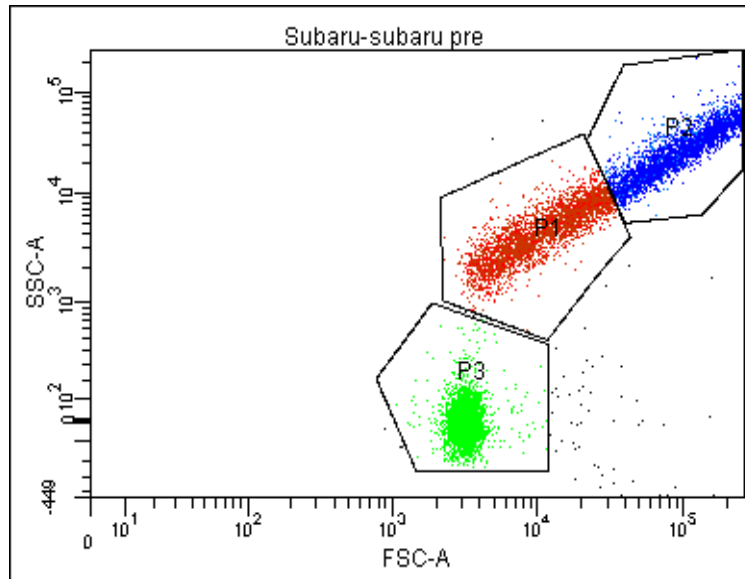
Figure C.7 Dot plot for Subaru pre-exerciser

Experiment Name:	sled dog blood sample				
Specimen Name:	Subaru				
Tube Name:	subaru pre				
Record Date:	Mar 28, 2013 8:37:43 PM				
$OP:	Administrator				
GUID:	ed025e64-3057-4579-8b84-8f63c788f3c8				

Population	#Events	%Parent	FSC-A Mean	SSC-A Mean	FITC-A Geo Mean
■ All Events	10,000	####	61,508	23,730	####
■ P1	3,081	30.8	13,149	4,957	####
■ P1'	1,696	55.0	13,479	5,031	6
■ P2	3,855	38.6	146,121	57,566	####
■ P2'	3,055	79.2	158,081	63,813	19
■ P3	3,015	30.2	3,222	-10	####

Figure C.8 Experiment data corresponds to Figure C.7

Figure C.9 Dot Plot for Subaru post-exercise

Population	#Events	%Parent	FSC-A Mean	SSC-A Mean	FITC-A Geo Mean
All Events	10,000	####	56,875	19,466	####
P1	3,567	35.7	13,150	4,749	####
P1'	1,802	50.5	13,611	4,845	6
P2	3,635	36.4	141,008	48,859	####
P2'	2,572	70.8	158,439	57,606	16
P3	2,774	27.7	3,158	-12	####

Experiment Name: sled dog blood sample
Specimen Name: Subaru
Tube Name: subraru post
Record Date: Mar 28, 2013 8:39:01 PM
$OP: Administrator
GUID: 84748b6d-b247-4704-a5c4-dcc7b07af82e

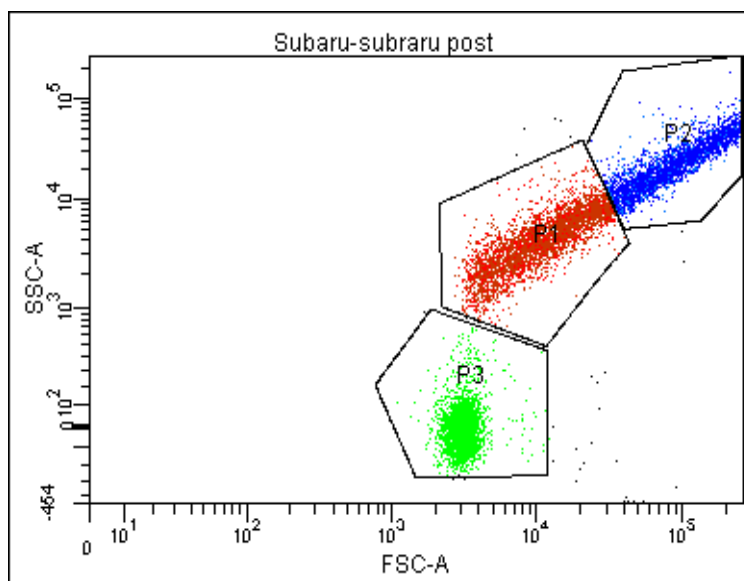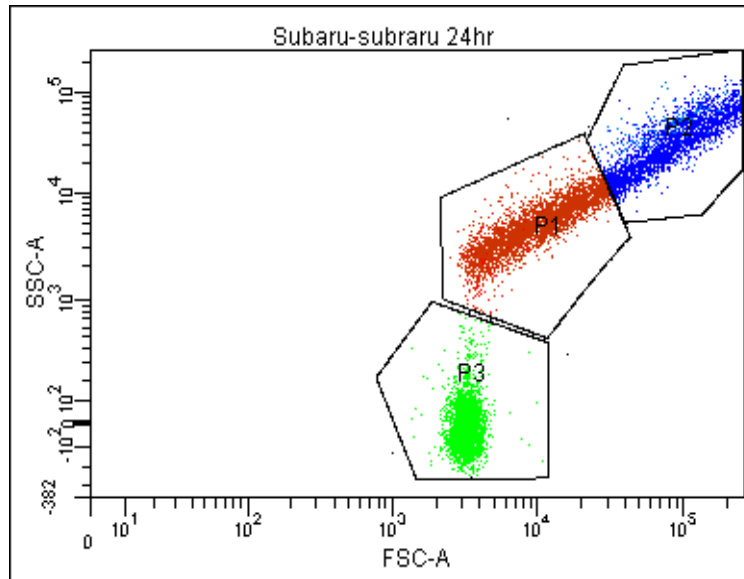**Figure C.10 Experiment data corresponds to Figure C.9**

Figure C.11 Dot plot for Subaru 24h-post exercise

Experiment Name: sled dog blood sample
Specimen Name: Subaru
Tube Name: subraru 24hr
Record Date: Mar 28, 2013 8:41:05 PM
$OP: Administrator
GUID: 1a226c01-3166-4c45-8570-cd4151d94e44

Population	#Events	%Parent	FSC-A Mean	SSC-A Mean	FITC-A Geo Mean
■ All Events	10,000	####	49,466	23,163	####
■ P1	3,420	34.2	11,869	5,661	####
■ P1'	3,019	88.3	12,324	5,810	9
■ P2	3,392	33.9	130,890	62,590	####
■ P2'	2,903	85.6	130,786	61,335	36
■ P3	3,186	31.9	3,222	-11	####

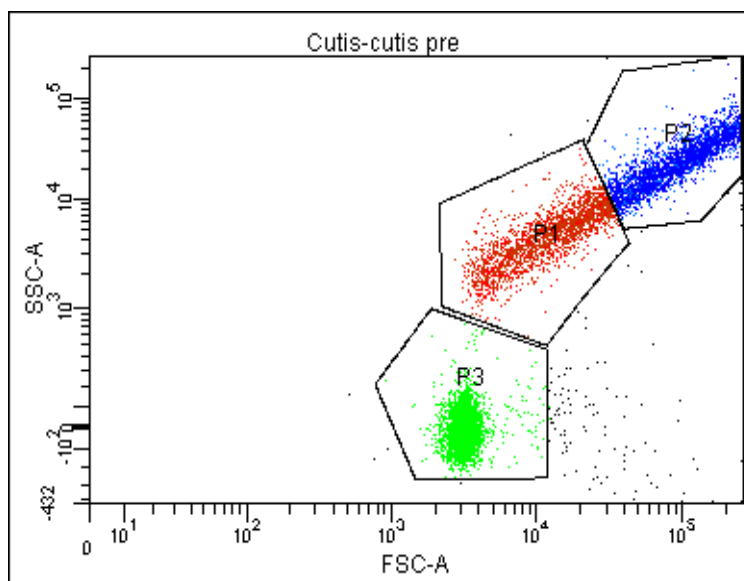**Figure C.12 Experiment data corresponds to Figure C.11**

Figure C.13 Dot plot for Curtis pre-exercise

Experiment Name:	sled dog blood sample
Specimen Name:	Cutis
Tube Name:	cutis pre
Record Date:	Mar 28, 2013 8:43:25 PM
$OP:	Administrator
GUID:	7f7cbc92-82d0-49fb-9b6e-aad1134f9887

Population	#Events	%Parent	FSC-A Mean	SSC-A Mean	FITC-A Geo Mean
■ All Events	10,000	####	83,188	34,750	####
■ P1	2,173	21.7	14,623	5,189	####
■ P1'	1,175	54.1	14,894	5,278	5
■ P2	4,603	46.0	170,364	72,954	####
■ P2'	3,342	72.6	177,964	76,372	13
■ P3	3,118	31.2	3,236	-8	####

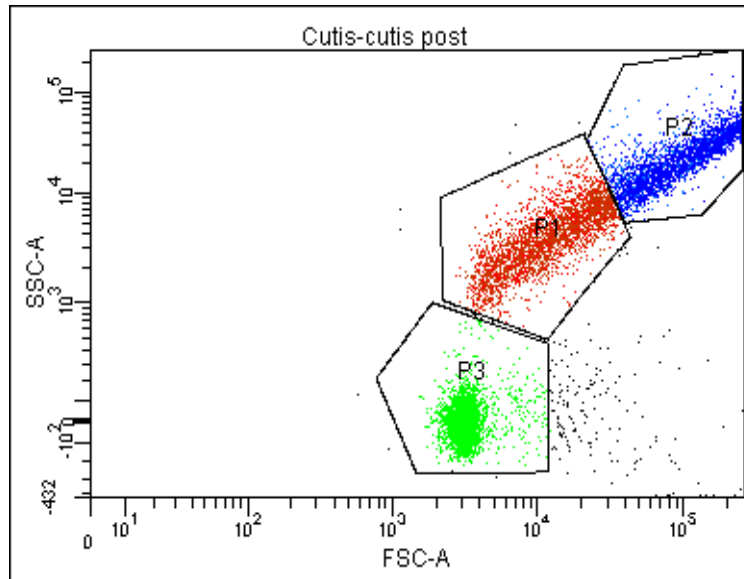**Figure C.14 Experiment data corresponds to Figure C.13**

Figure C.15 Dot plot for Curtis post-exercise

Experiment Name: sled dog blood sample
Specimen Name: Cutis
Tube Name: cutis post
Record Date: Mar 28, 2013 8:44:31 PM
$OP: Administrator
GUID: 295c487d-82c2-4e0b-8f18-73c7c264b95c

Population	#Events	%Parent	FSC-A Mean	SSC-A Mean	FITC-A Geo Mean
■ All Events	10,000	####	68,912	24,478	####
■ P1	2,831	28.3	14,254	4,652	####
■ P1'	1,650	58.3	14,401	4,596	5
■ P2	3,976	39.8	159,128	58,167	####
■ P2'	3,196	80.4	171,885	64,275	17
■ P3	3,025	30.2	3,358	-1	####

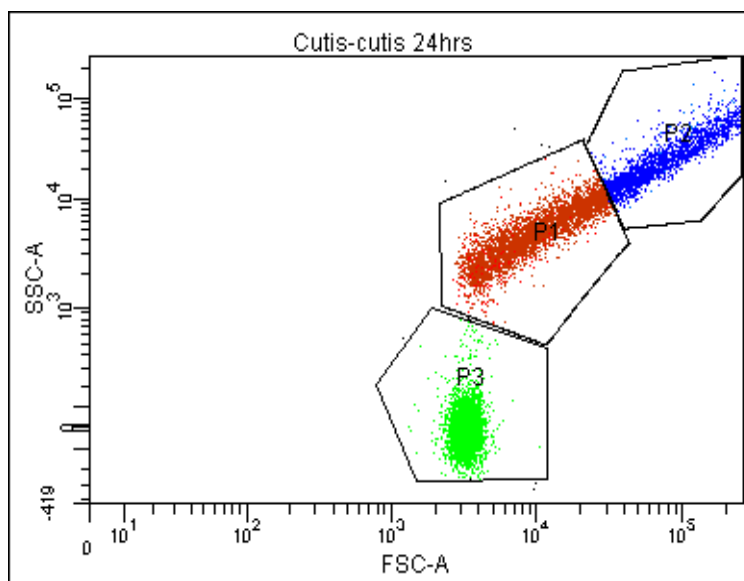**Figure C.16 Experiment data corresponds to Figure C.15**

Figure C.17 Dot plot for Curtis 24h-post exercise

Experiment Name: sled dog blood sample
Specimen Name: Cutis
Tube Name: cutis 24hrs
Record Date: Mar 28, 2013 8:45:57 PM
$OP: Administrator
GUID: 9db70e26-56a6-4fc0-ac19-a5295c15804f

Population	#Events	%Parent	FSC-A Mean	SSC-A Mean	FITC-A Geo Mean
■ All Events	10,000	####	31,468	11,330	####
■ P1	3,965	39.6	11,799	5,352	####
■ P1'	3,329	84.0	12,502	5,618	10
■ P2	2,325	23.2	110,237	39,609	####
■ P2'	2,245	96.6	110,363	39,230	50
■ P3	3,715	37.2	3,257	-11	####

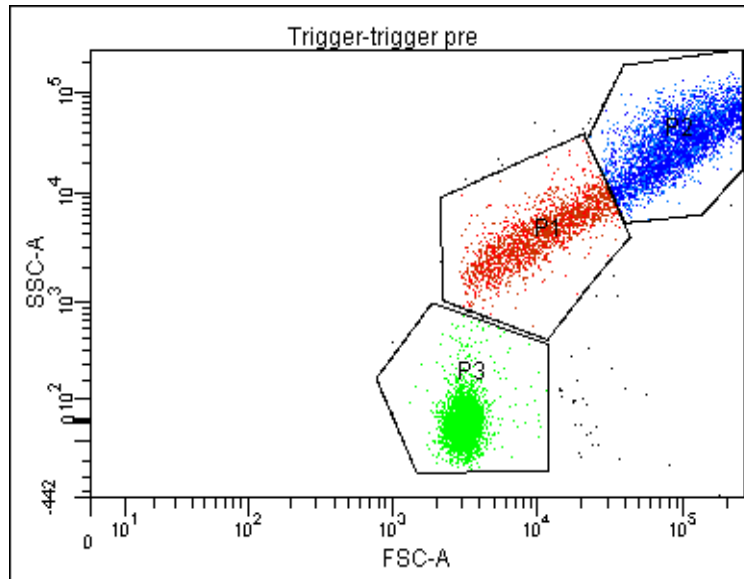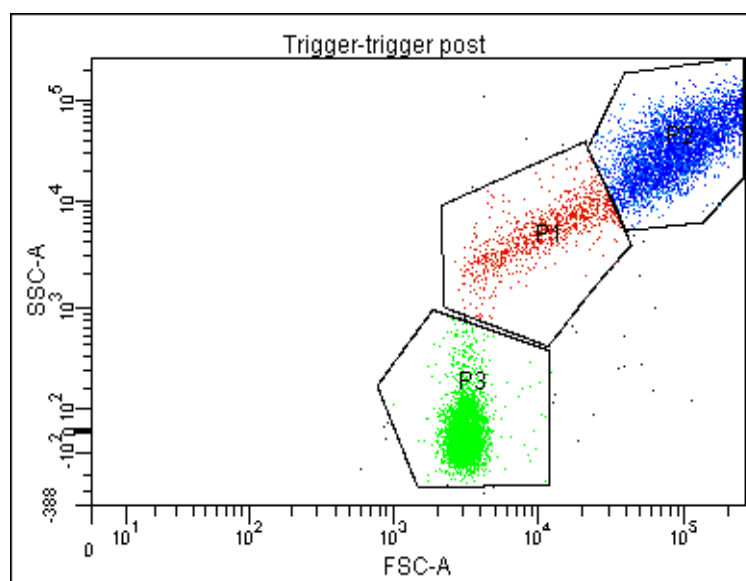**Figure C.18 Experiment data corresponds to Figure C.17**

Figure C.19 Dot plot for Trigger pre-exercise

Experiment Name: sled dog blood sample
Specimen Name: Trigger
Tube Name: trigger pre
Record Date: Mar 28, 2013 8:48:17 PM
$OP: Administrator
GUID: a6d7bc03-15bb-4b25-ac92-24620e78856f

Population	#Events	%Parent	FSC-A Mean	SSC-A Mean	FITC-A Geo Mean
All Events	10,000	####	69,863	30,576	####
P1	1,913	19.1	13,117	4,947	####
P1'	993	51.9	13,389	4,868	7
P2	4,691	46.9	141,121	63,090	####
P2'	2,568	54.7	156,121	73,424	15
P3	3,352	33.5	3,142	-8	####

Figure C.20 Experiment data corresponds to Figure C.19

Figure C.21 Dot plot for Trigger post-exercise

Experiment Name:	sled dog blood sample
Specimen Name:	Trigger
Tube Name:	trigger post
Record Date:	Mar 28, 2013 8:49:01 PM
$OP:	Administrator
GUID:	d931a19a-0741-4754-9db3-bc5d74de7bdd

Population	#Events	%Parent	FSC-A Mean	SSC-A Mean	FITC-A Geo Mean
All Events	10,000	####	73,355	33,791	####
P1	862	8.6	13,759	6,140	####
P1'	420	48.7	13,680	6,122	7
P2	5,168	51.7	137,034	64,223	####
P2'	2,421	46.8	150,312	75,554	12
P3	3,933	39.3	3,173	3	####

Figure C.22 Experiment data corresponds to Figure C.21
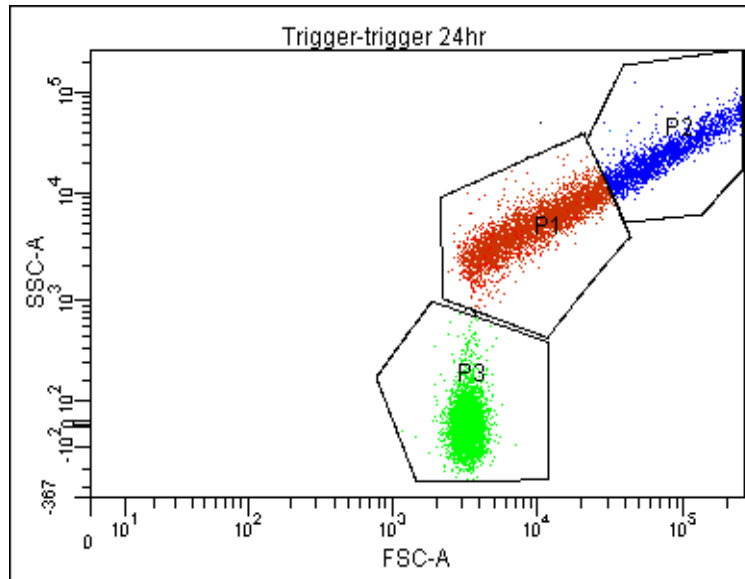
Figure C.23 Dot plot for Trigger 24h-post exercise

Population	#Events	%Parent	FSC-A Mean	SSC-A Mean	FITC-A Geo Mean
All Events	10,000	###	28,922	10,205	###
P1	3,691	36.9	11,633	5,541	###
P1'	2,982	80.8	12,376	5,816	9
P2	2,112	21.1	110,292	38,666	###
P2'	2,081	98.5	110,993	38,828	49
P3	4,203	42.0	3,273	-4	###

Experiment Name: sled dog blood sample
Specimen Name: Trigger
Tube Name: trigger 24hr
Record Date: Mar 28, 2013 8:49:52 PM
$OP: Administrator
GUID: 7005cea5-50fc-44a3-b515-9da711a71817

Figure C.24 Experiment data corresponds to Figure C.23
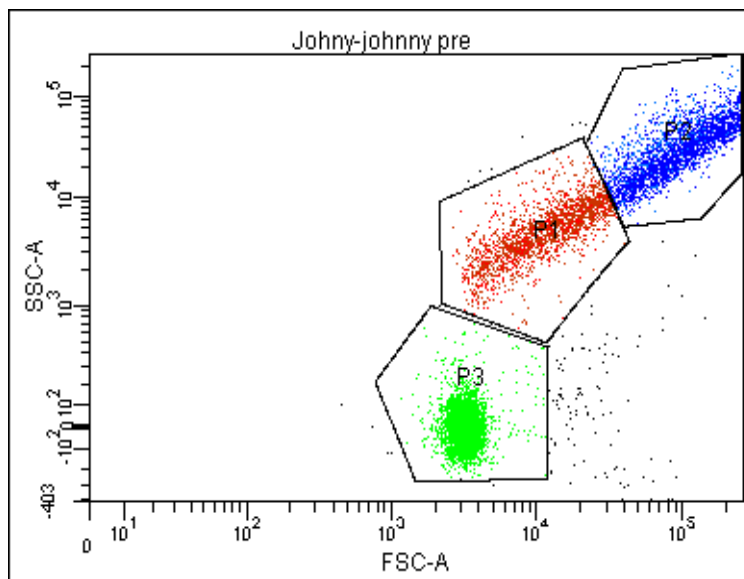
Figure C.25 Dot plot for Johnny pre-exercise

Experiment Name:	sled dog blood sample				
Specimen Name:	Johny				
Tube Name:	johnny pre				
Record Date:	Mar 28, 2013 8:59:09 PM				
$OP:	Administrator				
GUID:	7ed5159e-6ce8-48f4-8fbd-ce84c680a524				

Population	#Events	%Parent	FSC-A Mean	SSC-A Mean	FITC-A Geo Mean
All Events	10,000	####	66,662	30,026	####
P1	1,891	18.9	13,550	5,460	####
P1'	1,123	59.4	13,971	5,602	5
P2	3,864	38.6	161,585	74,987	####
P2'	2,947	76.3	173,334	81,530	15
P3	4,135	41.3	3,263	-4	####

Figure C.26 Experiment data corresponds to Figure C.25
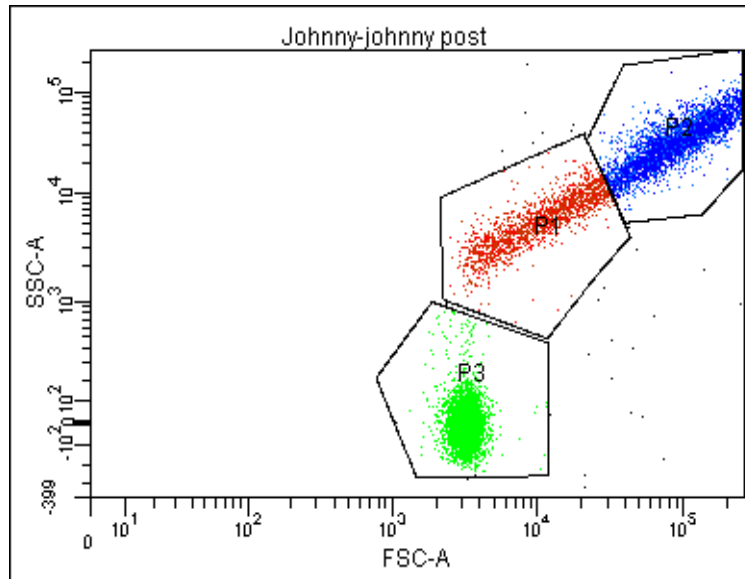
Figure C.27 Dot plot for Johnny post-exercise

Experiment Name:	sled dog blood sample
Specimen Name:	Johnny
Tube Name:	johnny post
Record Date:	Mar 28, 2013 9:00:17 PM
$OP:	Administrator
GUID:	31a67f04-d8a5-4e1a-b6aa-c89f7ae4f63a

Population	#Events	%Parent	FSC-A Mean	SSC-A Mean	FITC-A Geo Mean
■ All Events	10,000	####	66,252	28,569	####
■ P1	1,670	16.7	12,800	6,230	####
■ P1'	855	51.2	12,948	6,266	6
■ P2	4,426	44.3	141,806	62,040	####
■ P2'	2,502	56.5	155,442	71,339	13
■ P3	3,876	38.8	3,193	-4	####

Figure C.28 Experiment data corresponds to Figure C.27

Figure C.29 Dot plot for Johnny 24h-post exercise

Figure C.30 Experiment data corresponds to Figure C.29

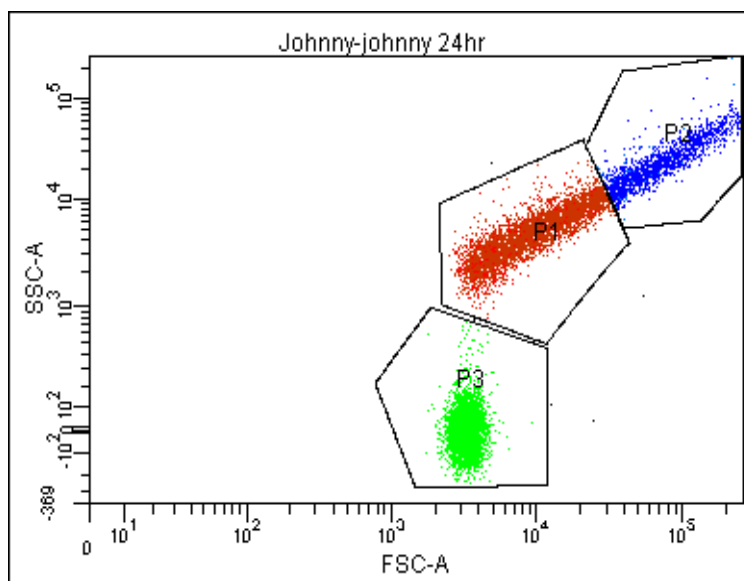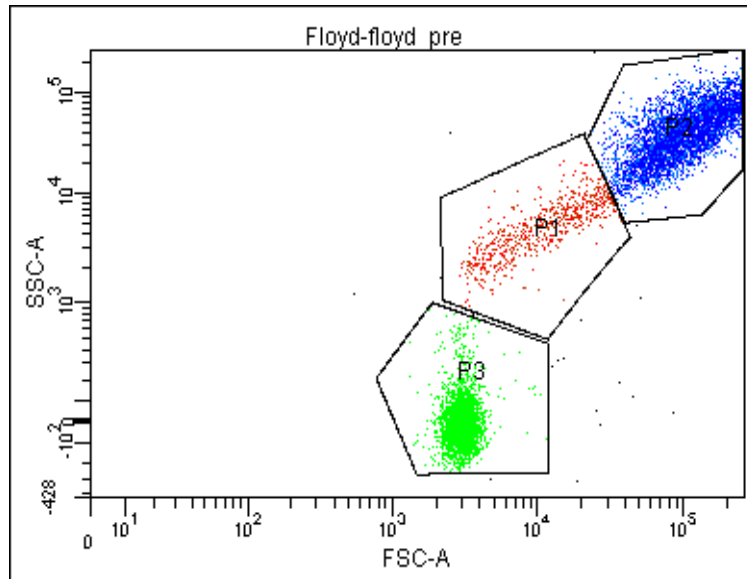**Figure C.31 Dot plot for Floyd pre-exercise**

Experiment Name: sled dog blood sample
Specimen Name: Floyd
Tube Name: floyd pre
Record Date: Mar 28, 2013 9:04:17 PM
$OP: Administrator
GUID: 3685e4dc-13ef-48bb-b806-c7ddecec888f

Population	#Events	%Parent	FSC-A Mean	SSC-A Mean	FITC-A Geo Mean
All Events	10,000	####	92,372	46,012	####
P1	675	6.8	13,471	5,527	####
P1'	376	55.7	13,877	5,593	5
P2	5,985	59.8	151,077	76,213	####
P2'	3,252	54.3	161,137	85,399	8
P3	3,321	33.2	3,034	-8	####

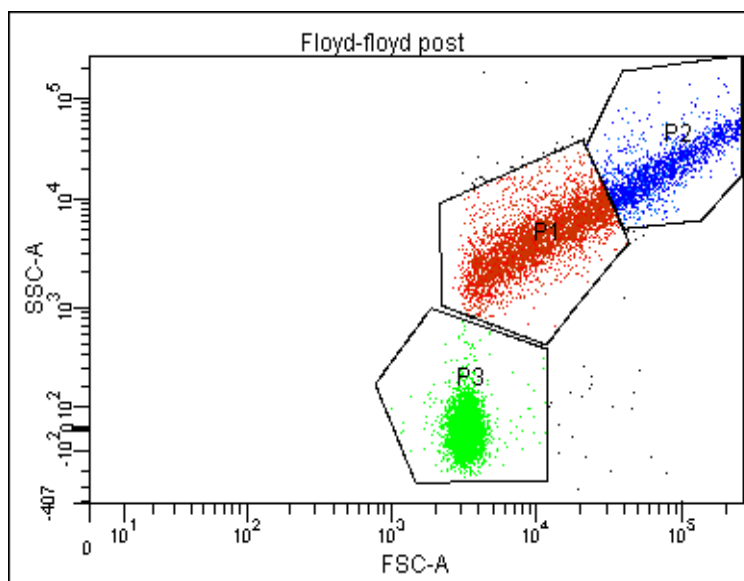**Figure C.32 Experiment data corresponds Figure C.31**

Figure C.33 Dot plot for Floyd post-exercise

Experiment Name: sled dog blood sample
Specimen Name: Floyd
Tube Name: floyd post
Record Date: Mar 28, 2013 9:05:36 PM
$OP: Administrator
GUID: 6bc0d03e-601d-4bdf-8598-a238d1ce185a

Population	#Events	%Parent	FSC-A Mean	SSC-A Mean	FITC-A Geo Mean
■ All Events	10,000	####	33,996	12,517	####
■ P1	3,936	39.4	12,400	5,027	####
■ P1'	2,344	59.6	12,905	5,164	5
■ P2	2,239	22.4	124,130	46,709	####
■ P2'	1,789	79.9	134,983	52,177	15
■ P3	3,779	37.8	3,280	-5	####

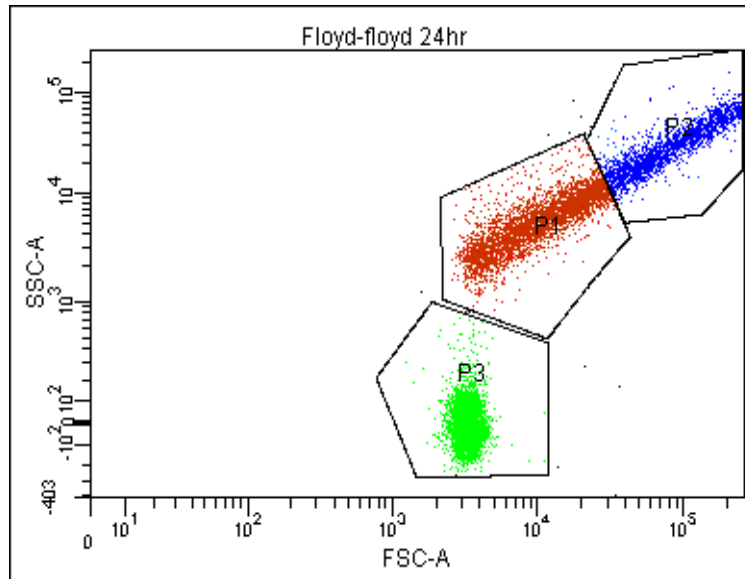**Figure C.34 Experiment data corresponds to Figure C.33**

Figure C.35 Dot plot for Floyd 24h-post exercise

Experiment Name:	sled dog blood sample
Specimen Name:	Floyd
Tube Name:	floyd 24hr
Record Date:	Mar 28, 2013 9:08:48 PM
$OP:	Administrator
GUID:	1f45e513-d10a-4fb4-8ece-e626ee5f15f6

Population	#Events	%Parent	FSC-A Mean	SSC-A Mean	FITC-A Geo Mean
All Events	10,000	####	34,553	13,817	####
P1	3,656	36.6	11,912	6,012	####
P1'	3,075	84.1	12,316	6,060	10
P2	2,388	23.9	121,024	48,557	####
P2'	2,295	96.1	123,203	49,336	58
P3	3,943	39.4	3,268	-8	####

Figure C.36 Experiment data corresponds to Figure C.35